

1 Inter-comparison of multiple two-way coupled meteorology and air quality models
2 (WRF v4.1.1-CMAQ v5.3.1, WRF-Chem v4.1.1, and WRF v3.7.1-CHIMERE v2020r1)
3 in eastern China

4
5 Chao Gao^{1,2}, Xuelei Zhang^{1,2,*}, Aijun Xiu^{1,2,*}, Qingqing Tong^{1,2}, Hongmei Zhao^{1,2}, Shichun Zhang^{1,2},
6 Guangyi Yang^{1,2,3}, Mengduo Zhang^{1,2,3}, and Shengjin Xie^{1,2,4}

7
8 ¹Key Laboratory of Wetland Ecology and Environment, Northeast Institute of Geography and Agroecology, Chinese
9 Academy of Sciences, Changchun, 130102, China

10 ²Key Laboratory of Wetland Ecology and Environment, State Key Laboratory of Black Soils Conservation and
11 Utilization, Northeast Institute of Geography and Agroecology, Chinese Academy of Sciences, Changchun, 130102,
12 China

13 ³University of Chinese Academy of Sciences, Beijing, 100049, China

14 ⁴School of Environment, Harbin Institute of Technology, 150000, Harbin, China

15 Correspondence to: X.L. Zhang (zhangxuelei@iga.ac.cn) & A.J. Xiu (xiujun@iga.ac.cn)

16
17 Abstract

18 *In the eastern China region, two-way coupled meteorology and air quality models*
19 *have been applied aiming to more realistically simulate meteorology and air quality by*
20 *accounting for the aerosol–radiation–cloud interactions. There have been numerous*
21 *related studies being conducted, but the performances of multiple two-way coupled*
22 *models simulating meteorology and air quality have not been compared in this region.*
23 *In this study, we systematically evaluated annual and seasonal meteorological and air*
24 *quality variables simulated by three open-source and widely used two-way coupled*
25 *models (i.e., WRF-CMAQ, WRF-Chem, and WRF-CHIMERE) by validating the model*
26 *results with surface and satellite observations for eastern China during 2017. Note that*
27 *although we have done our best to keep the same configurations, this study is not aiming*
28 *to screen which model is better or worse since different setups are still presented in*
29 *simulations. Our evaluation results showed that all three two-way coupled models*
30 *reasonably well simulated the annual spatiotemporal distributions of meteorological*
31 *and air quality variables. The impacts of aerosol-cloud interaction (ACI) on model*
32 *performances' improvements were limited compared to aerosol-radiation interaction*
33 *(ARI), and several possible improvements on ACI representations in two-way coupled*
34 *models are further discussed and proposed. When sufficient computational resources*
35 *become available, two-way coupled models should be applied for more accurate air*
36 *quality forecast and timely warning of heavy air pollution events in atmospheric*
37 *environmental management. The potential improvements of two-way coupled models*
38 *are proposed in future research perspectives.*

Formatted: Font: Italic, Font color: Blue

Formatted: Font: Italic, Font color: Blue

Formatted: Font: Italic

Formatted: Font: Italic, Font color: Blue

Formatted: Font: Italic

Deleted: In the eastern China region, Numerous two-way coupled meteorology and air quality models have been applied aiming to more realistically simulate investigate meteorology and air quality during severe air pollution periods in eastern China by accounting for the aerosol–radiation–cloud interactions. However, comprehensive assessments of There have been numerous related studies being conducted, but the performances of multiple two-way coupled models simulating long-term meteorology and air quality under equivalent configurations have not been compared conducted in this region. In this studyHere, we systematically evaluated annual and seasonal meteorological and air quality variables simulated by three open-source and widely used two-way coupled models (i.e., WRF-CMAQ, WRF-Chem, and WRF-CHIMERE) by validating the model results with surface and satellite observations for eastern China during 2017. Our comprehensiveThe model evaluations showed that all three two-way coupled models simulated the annual spatiotemporal distributions of meteorological and air quality variables reasonably well, especially the surface temperature (with R up to 0.97) and fine particular matter (PM_{2.5}) concentrations (with R up to 0.68). The model results of winter PM_{2.5} and summer ozone compared better with observations. The aerosol feedbacks affected model results of meteorology and air quality in various ways and turning on aerosol-radiation interactions made the PM_{2.5} and surface shortwave radiation simulations better, but worse for T2 and Q2. The impacts of aerosol-cloud interactions (ACI) on model performances' improvements were limited and several possible improvements on ACI representations in two-way coupled models are further discussed and proposed. When sufficient computational resources become available, two-way coupled models including the aerosol-radiation-cloud interactions should be applied for more accurate air quality prediction and timely warning of air pollution events in atmospheric environmental management.

Formatted: Font color: Blue

82 1 Introduction

83 Aerosols in the atmosphere due to anthropogenic and nature emissions not only
84 cause air pollution but also induce climate and meteorological impacts through aerosol-
85 radiation interaction (ARI) and aerosol-cloud interaction (ACI) (Carslaw et al., 2010;
86 Rosenfeld et al., 2014; Fan et al., 2016; IPCC, 2021). The feedbacks of aerosols to
87 meteorology have been widely investigated by two-way coupled meteorology and air
88 quality models in the past two decades (Jacobson, *1994, 1997, 1998, 2001*, 2002; Grell
89 et al., 2005; Wong et al., 2012; Wang et al., 2014; Zhou et al., 2016; Briant et al., 2017;
90 Feng et al., 2021). In these models, two-way interactions between meteorology and
91 aerosols are enabled by including all the processes involving ARI or/and ACI (Grell
92 and Baklanov, 2011; Wang et al., 2014; Briant et al., 2017; Wang et al., 2021). The
93 fundamental theories, modeling technics, developments, and applications of two-way
94 coupled meteorology and air quality models in North America, Europe and Asia have
95 been systemically reviewed (Zhang, 2008; Baklanov et al., 2014; Gao et al., 2022).

96 As pointed out by these review papers, the treatments and parameterization
97 schemes of all the physiochemical processes involving ARI and ACI can be very
98 different in two-way coupled models, so that the simulation results from these models
99 could vary in many aspects. At the same time, the configurations of coupled models,
100 such as meteorological and chemical initial and boundary conditions (ICs and BCs),
101 horizontal and vertical resolutions, and emission inventories and processing tools, etc.,
102 play important roles in models' simulations. In the past, model inter-comparison
103 projects have been carried out targeting various two-way coupled meteorology and air
104 quality models. For example, the Air Quality Model Evaluation International Initiative
105 Phase II focused on the performance of multiple two-way coupled models and the
106 effects of aerosol feedbacks in Europe and the United States (Brunner et al., 2015; Im
107 et al., 2015a, b; Makar et al., 2015a, b). In Asia, the Model Inter-Comparison Study for
108 Asia Phase III was conducted to evaluate ozone (O₃) and other gaseous pollutants, fine
109 particular matter (PM_{2.5}), and acid and reactive nitrogen deposition with various models
110 with/out ARI or/and ACI (Li et al., 2019; Chen et al., 2019; Itahashi et al., 2020; Ge et
111 al. al., 2020; Kong et al., 2020). With respect to this project, Gao et al. (2018, 2020)
112 have reviewed in detail the model performance of seven two-way coupled models from
113 different research groups in simulating a heavy air pollution episode during January
114 2010 in North China Plain and how aerosol feedbacks affected simulations of
115 meteorological variables and PM_{2.5} concentrations. Targeting the heavy polluted India
116 region, Govardhan et al. (2016) compared aerosol optical depth (AOD) and various
117 aerosol species (black carbon, mineral dust, and sea salt) modeled by WRF-Chem (with
118 ARI) and Spectral Radiation-Transport Model for Aerosol Species (with both ARI and
119 ACI), but under different model configurations.

120 So far, there is no comprehensive comparisons of multiple coupled models under
121 the same model configuration with respect to the high aerosol loading region over
122 eastern China, where has experienced rapid growth of economy, urbanization,
123 population, as well as severe air quality problems in the past decades (He et al., 2002;
124 Wang and Hao, 2012; Gao et al., 2017; Geng et al., 2021). In the eastern China region
125 (ECR), several open-source and proprietary two-way coupled models have been applied

Deleted:

127 to investigate the ARI and/or ACI effects, yet most studies have focused on certain
128 short-term episodes of heavy air pollution without any year-long simulations (Xing et
129 al., 2017; Ding et al., 2019; Ma et al., 2021). The commonly used open-source models
130 in ECR are WRF-Chem and WRF-CMAQ (Grell et al., 2005; Wong et al., 2012), but
131 there is no any application of the two-way coupled WRF-CHIMERE model that has
132 been applied to examine aerosol-radiation-cloud interactions in Europe and Africa
133 (Briant et al., 2017; Tuccella et al., 2019). At the same time, model simulations should
134 be compared not only against surface measurement data but also satellite data (Zhao et
135 al., 2017; Hong et al., 2017; Campbell et al., 2017; Wang et al., 2018). Even though the
136 running time of an individual modeling system (e.g., WRF-CMAQ and WRF-
137 CHIMERE) was evaluated by considering its online and offline versions and under
138 various computing configurations (Wong et al., 2012; Briant et al., 2017), the
139 computational efficiencies of multiple two-way coupled models need to be accessed
140 under the same computing conditions as well.

141 In this paper, a comparative evaluation of three open-sourced two-way coupled
142 meteorology and air quality models (WRF-CMAQ, WRF-Chem and WRF-CHIMERE)
143 in ECR is conducted. The remainder of the paper is organized as follows: Section 2
144 describes the study methods including model configurations and evaluation protocols.
145 Sections 3 and 4 presents the analyses and intercomparisons of simulations from these
146 three two-way coupled models with regard to meteorology and air quality, respectively.
147 The major findings of this work are summarized in Section 5.

148 2 Data and methods

149 2.1 Model configurations and data sources

150 One-year long-term simulations in eastern China were examined using the two-
151 way coupled WRF-CMAQ, WRF-Chem, and WRF-CHIMERE models, with and
152 without enabling ARI and/or ACI, and with 27-km horizontal grid spacing (there were
153 110, 120, and 120 grid cells in the east–west direction, and 150, 160, and 170 in the
154 north–south direction for WRF-CMAQ, WRF-Chem, and WRF-CHIMERE,
155 respectively). All the three coupled models used in this study have 30 levels (i.e., 29
156 layers) from the surface to 100 hPa with 11 layers in the bottom 1 km and the bottom-
157 layer thickness being 23.2 m. The anthropogenic emissions of Multi-resolution
158 Emission Inventory for China (MEIC) (Li et al., 2017) and the Fire INventory from
159 NCAR version 1.5 (FINN v1.5) biomass burning emissions (Wiedinmyer et al., 2011)
160 were applied in our simulations, and their spatial, temporal, and species allocations
161 were performed using Python language (Wang et al., 2023). Biogenic emissions were
162 calculated using the Model of Emissions of Gases and Aerosols from Nature version
163 3.0 (MEGAN v3.0) (Gao et al., 2019). Dust and sea-salt emissions were both used with
164 calculations of inline modules, as shown in Table 1. The meteorological ICs and lateral
165 BCs were derived from the National Center for Environmental Prediction Final
166 Analysis (NCEP-FNL) datasets (<http://rda.ucar.edu/datasets/ds083.2>), with a
167 horizontal resolution of $1^\circ \times 1^\circ$ at 6-hour intervals for each of the three coupled models,
168 and the flux in model-top boundary is set zero. To improve the long-term accuracy of
169

Commented [g1]: Wiedinmyer C, Akagi S K, Yokelson R J, et al. The Fire INventory from NCAR (FINN): A high resolution global model to estimate the emissions from open burning[J]. Geoscientific Model Development, 2011, 4(3): 625-641.

Commented [g2]: Wang K, Gao C, Wang H, et al. ISAT v2.0: An integrated tool for nested domain configurations and model-ready emission inventories for WRF-AQM[J]. Geoscientific Model Development Discussions, 2023: 1-18.

170 meteorological variables when using the WRF model, options of observational and grid
 171 four-dimensional data assimilation (FDDA) were turned on, and pressure, station height,
 172 relative humidity, wind speed, and wind direction were observed four times per day at
 173 00:00, 06:00, 12:00, and 18:00 UTC from 2168 stations
 174 (<https://doi.org/10.5281/zenodo.6975602>, Gao et al., 2022). *Tuning on FDDA in two-way*
 175 *coupled models could dampen the simulated aerosol feedbacks* (Wong et al., 2012;
 176 Forkel et al., 2012; Hogrefe et al., 2015; Zhang et al., 2016). *To reduce the effects of*
 177 *enabling FDDA on aerosol feedbacks in long-term simulations, here the nudging*
 178 *coefficients for u/v wind, temperature, and water vapor mixing ratio above the*
 179 *planetary boundary layer were set to 0.0001 s^{-1} , 0.0001 s^{-1} , and 0.00001 s^{-1} ,*
 180 *respectively. The chemical ICs/lateral BCs were downscaled from the Whole*
 181 *Atmosphere Community Climate Model (WACCM) for WRF-CMAQ and WRF-Chem*
 182 *via the moztart2camx and mozbc tools, respectively. WRF-CHIMERE used the*
 183 *climatology from a general circulation model developed at the Laboratoire de*
 184 *Météorologie Dynamique (LMDz) coupling a global chemistry and aerosol model*
 185 *Interactions between Chemistry and Aerosols (INCA) (Mailler et al., 2017). For*
 186 *chemical model-top BCs, WRF-CMAQ and WRF-Chem models both take into account*
 187 *the impacts of stratosphere-troposphere O_3 exchange using the parameterization of O_3 -*
 188 *potential vorticity (Safieddine et al., 2014; Xing et al., 2016), the related options for the*
 189 *two models were used in this study. In WRF-CHIMERE, the climatology from LMDz-*
 190 *INCA data was utilized (Mailler et al., 2017).*

191 The options of parameterization schemes of aerosol–radiation–cloud interactions
 192 are listed in Table 1. *To keep the consistency of physical schemes, the same RRTMG*
 193 *shortwave and longwave radiation schemes and Morrison microphysics schemes are*
 194 *adopted in both WRF-Chem and WRF-CMAQ. WRF-CHIMERE applied the same*
 195 *radiation schemes and Thompson microphysics scheme. The different other schemes*
 196 *(cumulus, surface, and land surface) in WRF-CMAQ and WRF-Chem were chosen*
 197 *according to widely used options outlined in Table S1 of Gao et al. (2022). The other*
 198 *schemes used in WRF-CHIMERE are the same as with WRF-Chem. To consider the*
 199 *effects of clouds on radiative transfer calculations, the fractional cloud cover and cloud*
 200 *optical properties were included in the RRTMG shortwave/longwave radiation schemes*
 201 *used by all three coupled models (Xu and Randall, 1996; Iacono et al., 2008). The*
 202 *coupled WRF-CMAQ model with the Kain-Fritsch cumulus scheme included the*
 203 *cumulus cloud fraction impacts on RRTMG radiation (Alapaty et al., 2012), but not the*
 204 *WRF-Chem and WRF-CHIMERE models with the Grell-Freitas cumulus scheme. In the*
 205 *Fast-JX photolysis scheme used by the three coupled models, the impacts of clouds are*
 206 *included by considering cloud cover and cloud optical properties. However, the*
 207 *calculations of cloud cover and cloud optical properties are different in these models*
 208 *and all the relevant information is listed in Table S1. As illustrated in Tables 1 and S2*
 209 *for aerosol size distribution, we used modal approach with Aitken, accumulation and*
 210 *coarse modes in WRF-CMAQ, and the 4-bin and 10-bin sectional approaches in WRF-*
 211 *Chem and WRF-CHIMERE models, respectively (Binkowski and Roselle, 2003; Zaveri*
 212 *et al., 2008; Nicholls et al., 2014; Menut et al., 2013, 2016).*

213 To demonstrate the capabilities of the three two-way coupled models with/without

Commented [g3]: Wong D C, Pleim J, Mathur R, et al. WRF-CMAQ two-way coupled system with aerosol feedback: software development and preliminary results[J]. Geoscientific Model Development Discussions, 2011, 4(3): 2417-2450.

Commented [g4]: Hogrefe C, Pouliot G, Wong D, et al. Annual application and evaluation of the online coupled WRF-CMAQ system over North America under AQMEII phase 2[J]. Atmospheric Environment, 2015, 115: 683-694.

Commented [g5]: Zhang Y, Zhang X, Wang K, et al. Application of WRF/Chem over East Asia: Part II. Model improvement and sensitivity simulations[J]. Atmospheric Environment, 2016, 124: 301-320.

Commented [g6]: Mailler S, Menut L, Khvorostyanov D, et al. CHIMERE-2017: From urban to hemispheric chemistry-transport modeling[J]. Geoscientific Model Development, 2017, 10(6): 2397-2423.

Commented [g7]: Safieddine S, Boynard A, Coheur P F, et al. Summertime tropospheric ozone assessment over the Mediterranean region using the thermal infrared IASI/MetOp sounder and the WRF-Chem model[J]. Atmospheric ...

Commented [g8]: Xing J, Mathur R, Pleim J, et al. Representing the effects of stratosphere-troposphere exchange on 3-DO 3 distributions in chemistry transport models using a potential vorticity-based parameterization[...]

Commented [g9]: Mailler S, Menut L, Khvorostyanov D, et al. CHIMERE-2017: From urban to hemispheric chemistry-transport modeling[J]. Geoscientific Model Development, 2017, 10(6): 2397-2423.

Commented [g10]: Xu K M, Randall D A. A semiempirical cloudiness parameterization for use in climate models[J]. Journal of the atmospheric sciences, 1996, 53(21): 3084-3102.

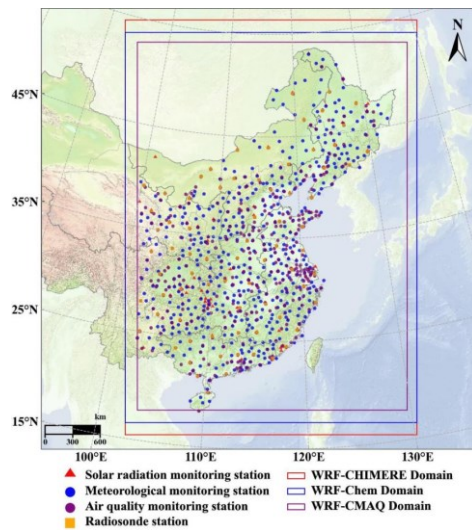
Commented [g11]: Iacono M J, Delamere J S, Mlawer E J, et al. Radiative forcing by long-lived greenhouse gases: Calculations with the AER radiative transfer models[J]. Journal of Geophysical Research: Atmospheres, 2008, ...

Commented [g12]: Alapaty K, Herwehe J A, Otte T L, et al. Introducing subgrid-scale cloud feedbacks to radiation for regional meteorological and climate modeling[J]. Geophysical Research Letters, 2012, 39(24).

214 feedbacks in simulating meteorology and air quality, we undertook comprehensive
 215 evaluations of the strengths and weaknesses each coupled model, validated against
 216 extensive ground-based and satellite measurements. Ground-based data included 572
 217 hourly ground-based meteorological observations (air temperature (T2) and relative
 218 humidity (RH2) air temperature at 2m above the surface, wind speed at 10m above the
 219 surface (WS10), and precipitation (PREC)) (<http://data.cma.cn>), 327 hourly national
 220 environmental observations (fine particulate matter (PM_{2.5}), ozone (O₃), nitrogen
 221 dioxide (NO₂), sulfur dioxide (SO₂), and carbon monoxide (CO))
 222 (<http://106.37.208.233:20035>), 109 hourly surface shortwave radiation (SSR)
 223 measurements (Tang et al., 2019) and 74 radiosonde sites retrieved twice per day (Guo
 224 et al., 2019); the locations of these data are depicted in Fig. 1. Because there were no
 225 observed water vapor mixing ratio (w) data, this parameter was calculated via the
 226 formula $w = \frac{rh}{w_s}$, where rh is the relative humidity and w_s is the saturation mixing ratio
 227 (Wallace and Hobbs, 2006).

228 Satellite data included the following: monthly average downwelling short-/long-
 229 wave flux at the surface and short-/long-wave flux at the top of the atmosphere (TOA)
 230 from the Clouds and the Earth's Radiant Energy System (CERES)
 231 (<https://ceres.larc.nasa.gov>); precipitation from the Tropical Rainfall Measuring
 232 Mission (TRMM); cloud fraction, liquid water path (LWP), and aerosol optical depth
 233 (AOD) from the Moderate Resolution Imaging Spectroradiometer (MODIS);
 234 tropospheric NO₂ column and SO₂ column in the planetary boundary layer (PBL) from
 235 the Ozone Monitoring Instrument (OMI); total CO column from the Measurements of
 236 Pollution in the Troposphere (MOPITT) (<https://giovanni.gsfc.nasa.gov/giovanni>);
 237 total column ozone (TCO) from the Infrared Atmospheric Sounding Interferometer-
 238 Meteorological Operational Satellite-A (IASI-METOP-A)
 239 (<https://cds.climate.copernicus.eu/cdsapp#!/dataset/satellite-ozone?tab=form>); and
 240 total ammonia (NH₃) column from IASI-METOP-B ([https://cds-](https://cds-espri.ipsl.fr/iasibl3/iasi_nh3/V3.1.0)
 241 espri.ipsl.fr/iasibl3/iasi_nh3/V3.1.0). These data were downloaded and interpolated to
 242 the same horizontal resolution as the model results using Rasterio library (Gillies et al.,
 243 2013), then the model and observed values at each grid point were extracted.

244



245

246 [Figure 1. Modeling domains \(WRF-CMAQ, WRF-Chem, and WRF-CHIMERE\), and solar](#)
 247 [radiation, meteorology, air quality, and radiosonde stations.](#)
 248
 249 [Table 1. Model setups and inputs for the two-way coupled models \(WRF-CMAQ, WRF-](#)
 250 [Chem and WRF-CHIMERE\).](#)

		WRF-CMAQ	WRF-Chem	WRF-CHIMERE
<i>Domain</i>	Horizontal grid spacing	27 km (110 × 150)	27 km (120 × 160)	27 km (120 × 170)
<i>configuration</i>	Vertical resolution	30 levels	30 levels	30 levels
<i>Physics</i>	Shortwave radiation	RRTMG	RRTMG	RRTMG
<i>parameterization</i>	Longwave radiation	RRTMG	RRTMG	RRTMG
	Cloud microphysics	Morrison	Morrison	Thompson
	PBL	ACM2	YSU	YSU
	Cumulus	Kain-Fritsch	Grell-Freitas	Grell-Freitas
	Surface	Pleim-Xiu	Monin-Obukhov	Monin-Obukhov
	Land surface	Pleim-Xiu LSM	Noah LSM	Noah LSM
	Icloud	Xu-Randall method	Xu-Randall method	Xu-Randall method
<i>Chemistry</i>	<i>Aerosol mechanism</i>	AERO6	MOSAIC	SAM
<i>scheme</i>	<i>Aerosol size distribution</i>	Modal (3 modes)	Sectional (4 bins)	Sectional (10 bins)
	<i>Aerosol mixing state</i>	Core-Shell	Core-Shell	Core-Shell
	<i>Gas-phase chemistry</i>	CB6	CBMZ	MELCHIOR2
	Photolysis	Fast-JX with cloud effects	Fast-JX with cloud effects	Fast-JX with cloud effects
<i>Emission</i>	Anthropogenic emission	MEIC 2017	MEIC 2017	MEIC 2017
	Biogenic emission	MEGAN v3.0	MEGAN v3.0	MEGAN v3.0
	Biomass burning emission	FINN v1.5	FINN v1.5	FINN v1.5
	Dust emission	Foroutan	GOCART	Menuet
	Sea-salt emission	Gong	Gong	Monahan
<i>Input data</i>	Meteorological ICs and BCs	FNL	FNL	FNL
	Chemical ICs and BCs	MOZART	MOZART	LMDZ-INCA

251
 252 [2.2 Scenario set up](#)
 253 [To thoroughly assess the performance of WRF v4.1.1-CMAQ v5.3.1, WRF-Chem](#)
 254 [v4.1.1, and WRF v3.7.1-CHIMERE v2020r1 and its affected by aerosol feedbacks over](#)
 255 [eastern during 2017, eight sets of annual hindcast simulations with/without ARI and/or](#)
 256 [ACI were conducted, as presented in Table 2. Compared to WRF v4.1.1-CMAQ v5.3.1](#)
 257 [and WRF-Chem v4.1.1, this version of WRF v3.7.1-CHIMERE v2020r1 can be](#)
 258 [officially obtained and the higher version of WRF-CHIMERE has not been developed.](#)
 259 [It should be noted that the officially released WRF-Chem and WRF-CHIMERE are](#)
 260 [capable of simulating ARI and ACI, but WRF-CMAQ is not. In all of the simulations](#)
 261 [performed in this study, a month of spin-up time was set up to reduce the influence of](#)
 262 [the initial conditions. Multiple statistical metrics between each scenario simulation and](#)
 263 [ground-based/satellite-borne observations were used including the correlation](#)
 264 [coefficient \(R\), mean bias \(MB\), normalized mean bias \(NMB\), normalized gross error](#)
 265 [\(NGE\), and root mean square error \(RMSE\). The mathematical definitions of these](#)

Deleted:

Moved (insertion) [1]: 2.2.2 Scenario set up
 To thoroughly assess the performance of WRF v4.1.1-CMAQ v5.3.1, WRF-Chem v4.1.1, and WRF v3.7.1-CHIMERE v2020r1 and its affected by aerosol feedbacks over eastern during 2017, Eight sets of annual hindcast WRF-CMAQ, WRF-Chem, and WRF-CHIMERE simulations with/without aerosol feedbacks ARI and/or ACI were carried out conducted to investigate the performance of each coupled model over eastern China during 2017, as presented in Table 22.
Compared to WRF v4.1.1-CMAQ v5.3.1 and WRF-Chem v4.1.1, this version of WRF v3.7.1-CHIMERE v2020r1 can be officially obtained and the higher version of WRF-CHIMERE has not been developed. It should be noted that the officially released WRF-Chem and WRF-CHIMERE are capable of simulating ARI and ACI, but WRF-CMAQ is not. In all of the simulations performed in this study, a month of spin-up time was set up to reduce the influence of the initial conditions.
 We calculated multiple model evaluation statistical metrics between each scenario simulation and relevant ground-based/satellite-borne observations were used including to assess the model performance; these included the correlation coefficient (R), mean bias (MB), normalized mean bias (NMB), *normalized gross error (NGE)*, and root mean square

Deleted: 2

Deleted: E

Deleted: WRF-CMAQ, WRF-Chem, and WRF-CHIMERE

Deleted: aerosol feedbacks...RI and/or ACI were carried to investigate the performance of each coupled model over

Deleted: carried out

Deleted: to investigate the performance of each coupled model over eastern China during 2017

Deleted: 2

Formatted: Font: Italic

Deleted: We calculated m...ultiple model between each scenario simulation and relevant...round-

Deleted: model evaluation

Deleted: relevant

Deleted: to assess the model performance; these included

Formatted: Font: Italic, Font color: Blue

392 metrics are provided in Supplement S1. To compare simulations by three coupled
 393 models, the respective model configurations of physics and chemistry routines are set
 394 as consistent as possible. We systemically analyzed the annual and seasonal statistical
 395 metrics of meteorological and air quality variables including simulations by all three
 396 two-way coupled models with/without enabling ARI and/or ACI effects. We then
 397 quantified the respective contributions of the ARI and ACI effects to model
 398 performance.

399 Table 2. Summary of scenarios setting in three coupled models.

Model	Scenario	Configuration option	Description
WRF-CMAQ	(1) WRF-CMAQ_NO	DO_SW_CAL=F	Without aerosol feedbacks
	(2) WRF-CMAQ_ARI	DO_SW_CAL=T	ARI
WRF-Chem	(3) WRF-Chem_NO	aer_ra_feedback=0 wetscav_onoff=0 cldchem_onoff=0	Without aerosol feedbacks
	(4) WRF-Chem_ARI	aer_ra_feedback=1 wetscav_onoff=0 cldchem_onoff=0	ARI
	(5) WRF-Chem_BOTH	aer_ra_feedback=1 wetscav_onoff=1 cldchem_onoff=1	ARI and ACI
WRF-CHIMERE	(6) WRF-CHIMERE_NO	direct_feed_chimere=0 indirect_feed_chimere=0	Without aerosol feedbacks
	(7) WRF-CHIMERE_ARI	direct_feed_chimere=1 indirect_feed_chimere=0	ARI
	(8) WRF-CHIMERE_BOTH	direct_feed_chimere=1 indirect_feed_chimere=1	ARI and ACI

400
 403 **3 Multi-model meteorological evaluations.**

404 This section presents annual and seasonal (March–April–May, Spring; June–July–
 405 August, Summer; September–October–November, Autumn; and December–January–
 406 February, Winter) statistical metrics of simulated meteorological variables and air
 407 quality when compared with ground-based and satellite observations, as well as a
 408 discussion of the running times of the eight scenario simulations.

409 **3.1 Ground-based observations**

410 Figures 2 and S1–S7 illustrate the spatial distributions of R, MB, and RMSE for
 411 hourly SSR, T2, Q2, RH2, WS10, PREC, PBLH00, and PBLH12 from WRF-CMAQ,
 412 WRF-Chem, and WRF-CHIMERE with/without turning on aerosol feedbacks against
 413 ground-based observations from each site across the whole of 2017. The calculated
 414 annual model evaluation metrics for all sites in eastern China are summarized in Table
 415 S1, and the related seasonal R and MB values are presented in Fig. 3. *Here, we mainly*
 416 *focused on the comparisons of SSR, T2, RH2, and WS10, and the analysis of PREC,*
 417 *PBLH00, and PBLH12 are presented in Section 1.1 of Supplement.*

Deleted: comprehensively

Deleted: Table 2... Summary of scenarios setting in three coupled models.

Deleted: 2

Formatted: Normal

Moved up [1]

Deleted: 2.1 Model configurations and data sources
 One-year long-term simulations in eastern China were examined using the two-way coupled WRF v4.1.1-CMAQ v5.3.1, WRF-Chem v4.1.1, and WRF v3.7.1-CHIMERE v2020r1 models, with and without enabling ARI and/or ACI, and with 27-km horizontal grid spacing (there were 110, 120, and 120 grid cells in the east–west direction, and 150, 160, and 170 in the north–south direction for WRF-CMAQ, WRF-Chem, and WRF-CHIMERE, respectively). The vertical resolution for all simulations consisted of 30 levels from the surface (~20 m) to 100 hPa. The anthropogenic emissions of Multi-resolution Emission Inventory for China (MEIC) (Li et al., 2017) and FINN v1.5 biomass burning emissions were applied in our simulations, and their spatial, temporal, and species allocations were performed using Python language. Biogenic emissions were calculated using the Model of Emissions of Gases and Aerosols from Nature version 3.0 (MEGAN v3.0) (Gao et al., 2019). Dust and sea-salt emissions were both used with calculations of inline modules, as shown in Table 1. The meteorological ICs and BCs were derived from the National Center for Environmental Prediction Final Analysis (NCEP-FNL) datasets (<http://rda.ucar.edu/datasets/ds083.2>), with a horizontal resolution of 1° × 1° at 6-hour intervals for each of the three coupled models. To improve the long-term accuracy of meteorological variables when using the WRF model, options of observational and grid four-dimensional data assimilation (FDDA) were turned on, and pressure, station height, relative humidity, wind speed, and wind direction were observed four times per day at 00:00, 06:00, 12:00, and 18:00 UTC from ...

Deleted: M

Deleted: and intercomparisons

Deleted: comparisons of

Deleted: ure

Formatted: Font: Italic

519 The accuracy of radiation predication is of great significance in evaluating ARI.
 520 Yearly and seasonal average simulated SSR data were compared with ground-based
 521 observations (Figs. 3 -4 and Table S3), and SSR over eastern China was simulated
 522 reasonably well by all models with R values in the range of 0.61–0.78. *All simulated*
 523 *results were overestimated at both annual and seasonal scales (MBs in spring and*
 524 *summer were larger than those in autumn and winter).* The overestimations of annual
 525 SSR were 19.98, 14.48, and 9.24 W m⁻² for WRF-CMAQ, WRF-Chem, and WRF-
 526 CHIMERE, respectively. Overestimations of SSR by most two-way coupled models
 527 were also reported for Europe and North America in the comparative study conducted
 528 by Brunner et al. (2015). Such overestimations could be explained by multiple factors,
 529 namely, the uncertainties in cloud development owing to PBL and convection
 530 parameterizations (Alapaty et al., 2012), and the diversity in treatment of land surface
 531 processes (Brunner et al., 2015), which appear to play more important roles than does
 532 the enabling of two-way aerosol feedbacks on SSR through ARI and ACI effects in the
 533 models. When the three models considered ARI effects, the simulation accuracy of SSR,
 534 over both the whole year and in the four seasons *were improved*, but the enabling of
 535 ACI effects resulted in relatively limited improvement. In addition, the MB variations
 536 of WRF-CMAQ and WRF-Chem simulations were higher in spring and winter than
 537 those in summer and autumn, while the MB of WRF-CHIMERE simulations showed a
 538 maximum in summer (–10.33 W m⁻²) and minimum in autumn (–7.64 W m⁻²). Both
 539 the annual and seasonal reductions in SSR simulated by WRF-Chem and WRF-
 540 CHIMERE with ACI effects enabled were much smaller than those with ARI effects
 541 enabled.

542 In general, the simulated magnitudes and temporal variations of air temperature at
 543 2 m above the ground showed a high order of consistency with observations (R = 0.88–
 544 0.97). *Looking at annual and seasonal T2, models tended to have a negative bias, and*
 545 *T2 underestimations in spring and winter were greater than those in summer and*
 546 *autumn (Figs. 3 and 4).* As pointed out by Makar et al. (2015a), WRF-CHEM and
 547 GEM-MACH gave negative MBs in summer and positive MBs in winter when both
 548 ACI and ARI effects were enabled, and WRF-CMAQ with only ARI effects enabled
 549 also produced negative MBs in summer over North America during 2010; note that the
 550 Makar et al (2015a) study lacked evaluations of meteorology in winter using WRF-
 551 CMAQ. The comparison results of MBs indicated that WRF-CHIMERE > WRF-
 552 CMAQ > WRF-Chem. The annual and seasonal MBs of WRF-CMAQ and WRF-Chem
 553 were approximately –1 °C, while those of WRF-CHIMERE ranged from –2 to –1 °C.
 554 The RMSEs were approximately equal for WRF-CMAQ (2.71–3.05 °C) and WRF-
 555 Chem (2.82–3.27 °C), and larger for WRF-CHIMERE (3.39–4.53 °C), at both annual
 556 and seasonal scales. It is noteworthy that underestimations of annual and seasonal T2
 557 were mitigated in eastern China in the three coupled models when ARI effects were
 558 enabled. When ACI effects were enabled, the MBs for T2 simulated by WRF-
 559 Chem_BOTH showed no significant changes compared with those of WRF-Chem_NO;
 560 WRF-CHIMERE_BOTH further enhanced the underestimations of T2 in the full year
 561 (–1.30 °C), spring (–0.12 °C), and winter (–0.40 °C) compared with WRF-
 562 CHIMERE_NO.

Deleted: explicitly

Deleted: *were*

Deleted: S1

Deleted: ;

Deleted: the

Formatted: Font: Italic, Font color: Blue

Formatted: Font: Italic, Font color: Blue

Formatted: Font: Italic, Font color: Blue

Deleted: *The overall model performances of WRF-CMAQ and WRF-Chem were better than that of WRF-CHIMERE, while*

Deleted: *a*

Deleted: they effectively improved

Deleted: and water vapor mixing ratio

Deleted: *(cool)*

Formatted: Font: Italic, Font color: Blue

Deleted: (BOTH)

Deleted: ,

577 Looking at RH2, annual and seasonal simulations using WRF-CMAQ had the
578 highest correlation with the observed values, followed by WRF-Chem, and WRF-
579 CHIMERE, and the smallest correlation coefficients for all three models occurred in
580 autumn (~ 0.5). The spatial MBs between simulations by the three models and
581 observations showed a general converse trend compared with T2 (i.e., RH2 was
582 overestimated where T2 was underestimated, and vice versa). This can be explained by
583 the calculation of RH2 being based on T2 in the models (Wang et al., 2021). The annual
584 and seasonal MBs were approximately 0.65%–71.03% and –21.30% to 60.00%,
585 respectively (Fig. 4 and Table S3), and only WRF-Chem produced negative MBs in
586 summer. The magnitude of RMSE showed an inverse pattern compared with R for all
587 three models, with maximum (28.48%–29.52%) and minimum (12.57%–16.07%)
588 values shown in autumn and summer, respectively. *As shown in Figs. 3, 4 and Table S3,*
589 *WRF-CMAQ_ARI further reduced the overestimations of annual and seasonal RH2 in*
590 *eastern China, while WRF-Chem_ARI (except for summer) and WRF-CHIMERE_ARI*
591 *showed the opposite trend.* Moreover, variations in annual and seasonal RH2 MBs
592 simulated by WRF-Chem_BOTH and WRF-CHIMERE_BOTH were further reduced
593 compared with WRF-Chem_ARI (except for summer) and WRF-CHIMERE_ARI,
594 respectively.

595 Similar analyses were also performed for WS10, and revealed that WRF-CMAQ
596 performed better in capturing WS10 patterns compared with WRF-Chem and WRF-
597 CHIMERE. *The R values for all three models ranged from 0.47 to 0.60; WRF-CMAQ*
598 *and WRF-Chem overestimated wind speed by approximately 0.5 m s⁻¹, while WRF-*
599 *CHIMERE overestimated it by approximately 1.0 m s⁻¹ (Table S3 and Figs. 3, 4).* The
600 overestimation of WS10 under real-world low wind conditions is a common
601 phenomenon of current weather models, which is mainly caused by outdated
602 geographic data, coarse model resolution, and a lack of a good physical representation
603 of the urban canopy (Gao et al., 2015, 2018). All three models presented lower
604 correlations (0.31–0.54) and MBs (0.20–0.86 m s⁻¹) in summer compared with other
605 seasons, and the RMSEs were approximately 2.0 m s⁻¹. When ARI effects were enabled,
606 the overestimations of the three models were alleviated, especially for WRF-
607 CMAQ_ARI.

608

Deleted: For Q2, WRF-CMAQ showed the best performance, followed by WRF-Chem, and WRF-CHIMERE (Table S1 and Figure S2), all with RMSEs of less than 3 g kg⁻¹. Most models tended to underestimate annual and seasonal Q2 (–0.57 to –0.18 g kg⁻¹ and –1.16 to +0.20 g kg⁻¹, respectively), and the underestimations were most significant in summer. However, multiple two-way coupled models produced slightly positive values for Q2 during January 2010 over the North China Plain in the MICS-Asia III project (Gao et al., 2018). Compared with simulations that did not have aerosol feedbacks enabled, WRF-CMAQ_ARI and WRF-CHIMERE_ARI increased the negative biases of annual and seasonal Q2, with the former being more significant (Figure 3 and Table S1). The changes in annual, summer, and autumn MBs for WRF-Chem_ARI were consistent with the trend of WRF-CMAQ_ARI, except for spring and winter.

Deleted: Figure

Deleted: 3

Deleted: S1

Deleted: ure

Deleted: SI

Formatted: Font: Italic, Font color: Blue

Formatted: Font: Italic, Font color: Blue

Formatted: Font: (Default) Times New Roman, Italic, Font color: Blue

Formatted: Font: Italic, Font color: Blue

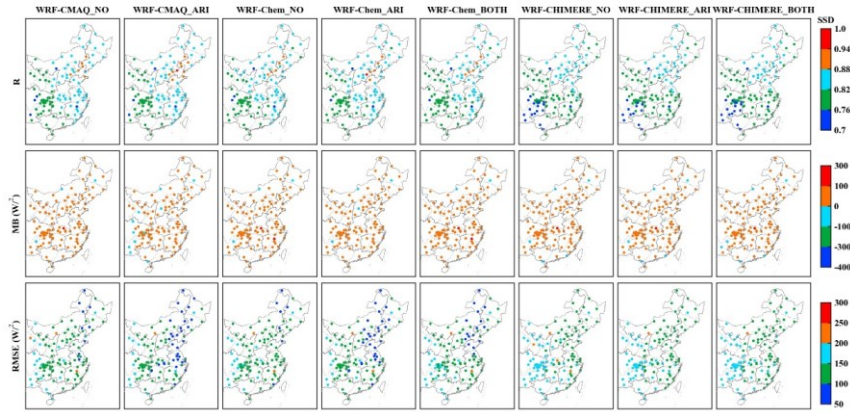
Formatted: Font: Italic, Font color: Blue

Formatted: Font: Italic

Formatted: Font: Italic, Font color: Blue

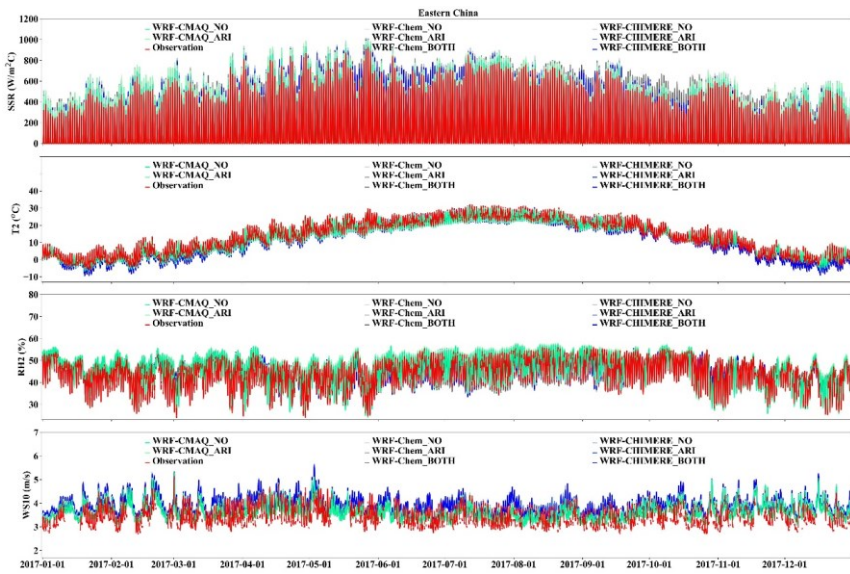
Deleted: Gao et al., 2015; Gao et al., 2018

Deleted: The annual and seasonal correlation coefficients of precipitation were 0.56–0.69, 0.46–0.63, and 0.25–0.55 for WRF-CMAQ, WRF-Chem, and WRF-CHIMERE, respectively (Table S1 and Figure S5). All simulated results had the highest correlations in winter and the lowest in summer, because the convective activity was enhanced in summer and the models struggle to effectively capture this. WRF-CMAQ and WRF-CHIMERE (WRF-Chem except for autumn) underestimated and overestimated annual and seasonal precipitation, respectively. At the annual and seasonal scales, WRF-Chem and WRF-CHIMERE overestimated the magnitude of daily precipitation by more than 1 mm day⁻¹, while WRF-CMAQ underestimated it by ...



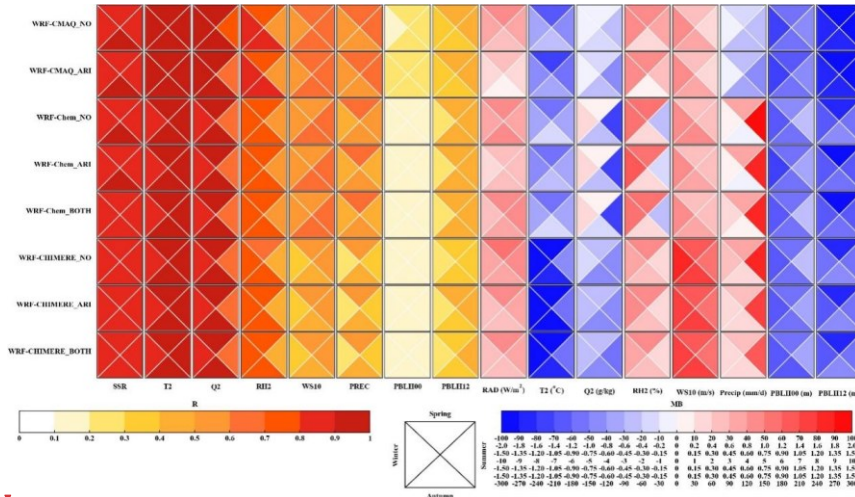
698

699 Figure 2. Statistical metrics (R, MB, and RMSE) between annual simulations and observations of
 700 surface shortwave radiation in eastern China.



701

702 *Figure 3. Time series of observed and simulated hourly SSR, T2, RH2 and WS10 by*
 703 *coupled WRF-CMAQ, WRF-Chem and WRF-CHIMERE with/without aerosol*
 704 *feedbacks over Eastern China during the year of 2017.*



Deleted:

705

706 Figure 4. Portrait plots of statistical indices (R and MB) between seasonal simulations and surface
 707 observations of meteorological variables (SSR, T2, Q2, RH2, WS10, PREC, and PBLH at LT 08:00
 708 and 20:00) in eastern China.

Deleted: 3

709 To identify and quantify how well our results compare with previous studies using
 710 two-way coupled models, we here discuss comparisons between our work and earlier
 711 research in terms of the evaluation results of meteorology and air quality; meteorology
 712 is discussed in this section and air quality is discussed in Section 4.1. Box-and-whisker
 713 plots were used and the 5th, 25th, 75th, and 95th percentiles were used as statistical
 714 indicators. In the plots, the dashed lines in the boxes are the mean values, and the circles
 715 represent outliers. Previous studies mainly used WRF-Chem and WRF-CMAQ to
 716 evaluate meteorology and air quality, while applications of WRF-NAQPMS and
 717 GRAPES-CUACE were scarce. As mentioned in Section 1, investigations of
 718 meteorology and air quality using WRF-CHIMERE with/without aerosol feedbacks
 719 have not previously been conducted in eastern China. Therefore, only evaluation results
 720 involving WRF-Chem and WRF-CMAQ to study aerosol feedbacks are analyzed herein.

Deleted:

721 The statistical metrics of T2, RH2, Q2, and WS10 in this study compared with the
 722 evaluation results of previous studies are presented in Fig. S8. According to the number
 723 of samples (NS) in the statistical metrics of each meteorological variable, most previous
 724 studies mainly involved the simulation and evaluation of T2, WS10, and RH2, with
 725 relatively few studies focusing on Q2. Compared with the evaluation results of previous
 726 studies, the ranges of statistical metrics in our study were roughly similar, but there
 727 were some important differences. The R values of the WRF-CMAQ and WRF-Chem
 728 models in our study were higher than those of previous studies; the MBs of T2 simulated
 729 via WRF-CMAQ were smaller, but those of T2 simulated via WRF-Chem were larger;
 730 and the RMSEs of the WRF-CMAQ simulation were larger, but those of the WRF-
 731 Chem simulation were smaller. For RH2, the R values for WRF-CMAQ and WRF-
 732 Chem in this study were all larger than the average level of previous studies, while the
 733 MBs and RMSEs for WRF-CMAQ were larger, and those for WRF-Chem were smaller

Deleted: Figure 4 illustrates t

739 than the average of previous studies. For Q2, the model performance of WRF-CMAQ
 740 in this study was generally better than the average level of previous studies, but the R
 741 between WRF-Chem simulation results and observed values was higher (and MB and
 742 RMSE were lower) than the average level of previous studies. We also conclude that
 743 the simulation results of WRF-CMAQ and WRF-Chem in our study better reproduced
 744 variations in WS10 compared with previous studies.

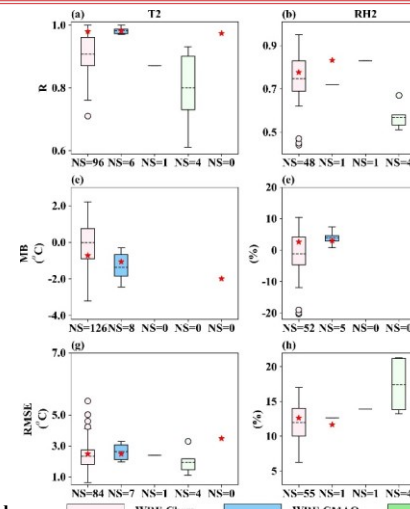
746 3.2 Satellite-borne observations

747 *To further evaluate the performance of WRF-CMAQ, WRF-Chem, and WRF-*
 748 *CHIMERE against satellite observations, we analyzed the annual and seasonal*
 749 *statistical metrics of short- and long-wave radiation at the surface, precipitation, cloud*
 750 *cover, and liquid water path simulated by the three coupled models with and without*
 751 *aerosol feedbacks, via comparisons between simulations and satellite-borne*
 752 *observations (Table 3; Figures 5, S9, S12–S14). In addition, the evaluations of short-*
 753 *and long-wave radiation at top of the atmosphere (TOA) are presented in Section 1.2*
 754 *of Supplement.*

755 *As shown in Table 3 and Fig. 5, the three coupled models showed relative poor*
 756 *performance for the shortwave radiation variables at the surface (SSR) annual MBs of*
 757 *8.21–30.74 W m⁻², and correlations ranging from 0.61 to 0.78. A similar poor*
 758 *performance for shortwave radiation was also reported in the USA using the coupled*
 759 *WRF-CMAQ and offline WRF models (Wang et al., 2021). The overall seasonal*
 760 *characteristics of SSR were successfully reproduced by the three coupled models (Fig.*
 761 *S10). Meanwhile, no matter whether aerosol feedbacks were enabled or not, all three*
 762 *models overestimated seasonal SSR (except for WRF-Chem ARI in winter), and*
 763 *showed higher MBs in spring and summer than in autumn and winter. The seasonal*
 764 *SSR overestimations may be a direct result of the underestimation of calculated AOD*
 765 *when considering ARI effects (Wang et al., 2021). Compared to SSR, the three coupled*
 766 *models predicted the longwave radiation variables at the surface (SLR) well (R values*
 767 *up to 0.99), with annual domain-average MBs of –9.97 to –6.05 W m⁻². Significant*
 768 *seasonal differences in simulated longwave radiation were also present among the three*
 769 *coupled models; all WRF-CMAQ and WRF-CHIMERE scenarios gave*
 770 *underestimations, with maximum and minimum values of SLR in winter and summer,*
 771 *respectively, while the maximum underestimations of WRF-Chem occurred in autumn,*
 772 *especially for WRF-Chem_BOTH (Fig. S9).*

773 *As all three coupled models adopted the same grid resolution (27 × 27 km) and*
 774 *short- and long-wave radiation schemes (RRTMG), the above analysis demonstrated*
 775 *that the representation differences for aerosol components, size distributions and*
 776 *mechanisms contributed to the diversity of seasonal MBs (Tables 1 and S2). Moreover,*
 777 *the three two-way coupled models with ARI feedbacks enabled effectively improved*
 778 *the performances of annual and seasonal SSR; however, for SLR, performance*
 779 *improvements were much more variable across the three coupled models and across*
 780 *different scenarios with and without ARI and/or ACI feedbacks enabled (Table S4).*
 781 *When ARI effects are enabled, the diversities of refractive indices of aerosol species*
 782 *groups lead to the discrepancies of online calculated aerosol optical properties in*

Deleted: (Fig. 4d)



Deleted:

Figure 4. Comparisons of model capacities between our study (red stars) and previous literature (box plots) in terms of the surface T2, RH2, Q2, and WS10 in eastern China. Note that red stars in the fifth column of each subgraph represent the statistical metrics of WRF-CHIMERE in this study.

Formatted: Font: Italic

Moved (insertion) [2]: Compared with longwave radiationAs shown in Table 3 and Fig. 5, the three coupled models showed relative poorer performance for the shortwave radiation variables at the surface (SSR) and top of the atmosphere (TSR) with annual MBs of 8.21–30.74 W m⁻² and –4.40 to +5.42 W m⁻², respectively, and correlations

Deleted: To further evaluate the wider spatial performance of WRF-CMAQ, WRF-Chem, and WRF-CHIMERE, we analyzed the annual and seasonal statistical metrics of short- and long-wave radiation at the surface and top of the

Deleted: er...performance for the shortwave radiation variables at the surface (SSR) and top of the atmosphere (TSR) with ...nnual MBs of 8.21–30.74 W m⁻² and –4.40 to +5.42 W m⁻², respectively... and correlations ranging from...

Moved up [2]

Deleted: s...that the representation differences for aerosol components, size distributions and mechanisms contributed to the diversity of seasonal MBs (Tables 1 and S2),the configurations of different aerosol/gas chemical mechani...

Formatted

059 *different shortwave and longwave (SW and LW) bands in the RRTMG SW/LW radiation*
060 *schemes of WRF-CMAQ, WRF-Chem, and WRF-CHIMERE (Tables S5–S6). The online*
061 *calculated cloud optical properties induced by aerosol absorption in the RRTMG*
062 *radiation schemes are different in treatments of aerosol species groups in the three*
063 *coupled models. With enabling ACI effects, the activation of cloud droplets from*
064 *aerosols based on the Köhler theory is taken into account in WRF-Chem and WRF-*
065 *CHIMERE, in comparison to simulations without aerosol feedbacks (Table S7). The*
066 *treatments of prognostic ice nucleating particles (INP) formed via heterogeneous*
067 *nucleation of dust particles (diameters > 0.5 μm) and homogeneous freezing of*
068 *hygroscopic aerosols (diameters > 0.1 μm) are only considered in WRF-CHIMERE,*
069 *but the prognostic ice nucleating particles are not included in WRF-CMAQ and WRF-*
070 *Chem. These discrepancies eventually contribute to the differences of simulated*
071 *radiation changes caused by aerosols.*

Formatted: Font: Italic, Font color: Blue

1072 From IPCC 2007 to IPCC 2021, the effects of aerosol feedbacks (especially for
1073 ACI effects) on precipitation and cloud processes remain under debate. Here, we further
1074 assessed annual and seasonal simulated precipitation, cloud cover, and liquid water
1075 pathways in eastern China with high aerosol loadings against satellite observations
1076 (Table 3 and Figs. S12–S14), and attempted to provide new insights from a yearly
1077 perspective into enabling online feedbacks in two-way coupled modeling simulations.

Deleted: Figures

Deleted: S11

Deleted: 3

Deleted: that

1078 The results illustrated those correlations of precipitation via WRF-CMAQ (0.51–
1079 0.89) were larger than those of WRF-Chem (0.61–0.73) and WRF-CHIMERE (0.54–
1080 0.70). WRF-CMAQ had the best correlation in winter, while WRF-Chem and WRF-
1081 CHIMERE had the best correlation in spring; all three models showed their worst
1082 correlation in summer. The reason for this is that numerical models struggle to
1083 effectively capture enhanced convective activity in summer. Huang and Gao (2018)
1084 also pointed out that accurate representations of lateral boundaries are crucial in
1085 improving precipitation simulations during summer over China. WRF-CMAQ
1086 underestimated annual precipitation, with MBs of –76.49 to –51.93 mm, while WRF-
1087 Chem and WRF-CHIMERE produced large precipitation overestimations ranging from
1088 +108.04 to +207.05 mm (Table 3), especially in regions of southern China (Fig. S11).
1089 WRF-CMAQ also produced negative biases (–27.89 to +42.08 mm) of seasonal
1090 precipitation, excluding WRF-CMAQ_ARI in winter. WRF-Chem and WRF-
1091 CHIMERE only underestimated seasonal precipitation in autumn (–31.39 to –26.89
1092 mm) and winter (–7.12 to –4.43 mm), respectively (Fig. S12). The variations in annual
1093 and seasonal MBs of precipitation were consistent with changes in cloud fraction and
1094 LWP (Zhang et al., 2016), which will be discussed in more detail below.

Deleted: ure

Deleted: Figure

Deleted: S11

1095 When aerosol feedbacks were considered, the ARI-induced reductions in the
1096 annual MBs of precipitation for WRF-CMAQ, WRF-Chem, and WRF-CHIMERE were
1097 24.56, 12.11, and 4.70 mm, respectively. WRF-Chem_BOTH (24.9 mm) and WRF-
1098 CHIMERE_BOTH (3.41 mm) enhanced the overestimation of annual precipitation
1099 compared with WRF-Chem_ARI and WRF-CHIMERE_ARI, respectively. Significant
1100 increases (+53.15 mm) and decreases (–6.3 to –3.41 mm) in MBs in winter and summer,
1101 respectively, were produced by WRF-CMAQ and the other two models with ARI effects
1102 enabled compared with no feedbacks. WRF-Chem and WRF-CHIMERE with both ARI

1110 and ACI effects enabled led to larger enhancements of MBs (+3.54 to +7.46) at the
1111 seasonal scale (Fig. S12). It must be noted that the discrepancies in simulated
1112 precipitation could mainly be attributed to the selection of different microphysics and
1113 cumulus schemes in WRF-CMAQ (Morrison and Kain-Fritsch), WRF-Chem (Morrison
1114 and Grell-Freitas), and WRF-CHIMERE (Thompson and Grell-Freitas).

1115 Cloud fraction (CF) and LWP can significantly influence the spatiotemporal
1116 distributions of precipitation; our simulated results of annual and seasonal CF over
1117 eastern China are presented in Table 3 and Fig. S13. Overall, WRF-CMAQ performed
1118 best in simulating CF. The R values for WRF-Chem during summer (0.69) and winter
1119 (0.70) were larger than those of WRF-CMAQ (0.59 and 0.64) and WRF-CHIMERE
1120 (0.56 and 0.66), while WRF-CMAQ and WRF-CHIMERE showed better simulation
1121 results in winter and autumn with correlations of up to 0.89 and 0.67, respectively. All
1122 three coupled models underestimated annual and seasonal CF with MBs that ranged
1123 from -16.83% to -6.18% and -21.13% to -4.13%, respectively; these were consistent
1124 with previous two-way coupled modeling studies using WRF-CMAQ (-19.7%) and
1125 WRF-Chem (-32% to -9%) in China (Hong et al., 2017; Zhao et al., 2017). All models
1126 reasonably simulated annual LWP in eastern China, with R values above 0.55 and
1127 negative biases varying from -57.36 to -31.29 g m⁻². The underestimations were
1128 closely related to missing cloud homogeneity (Wang et al., 2015; Dionne et al., 2020)
1129 and excessive conversion of liquid to ice in all selected cloud microphysics schemes
1130 (Klein et al., 2009). As shown in Fig. S14, all models showed their best performance in
1131 simulating LWP in spring (R = 0.51-0.79) and exhibited the largest underestimations
1132 in winter (MBs of -54.82 to -40.89 g m⁻²), except for WRF-Chem, which had its
1133 maximum bias in autumn.

1134 In terms of quantitatively determining the functions of aerosol feedbacks on CF
1135 and LWP, all simulated scenarios revealed that WRF-CMAQ_ARI overwhelmingly
1136 decreased annual and seasonal underestimations of CF (0.48%-1.05%) and LWP (3.03-
1137 4.29 g m⁻²), while there were slightly increased underestimations (CF: 0.02%-0.39%;
1138 LWP: 0.03-0.58 g m⁻²) in WRF-Chem_ARI and WRF-CHIMERE_ARI. Larger
1139 variations in annual and seasonal MBs of CF (0.23%-0.93%) and LWP (-2.96 g m⁻² to
1140 7.38 g m⁻²) were produced by WRF-CHIMERE_BOTH compared with WRF-
1141 CHIMERE_ARI. WRF-Chem_BOTH showed equivalent variations (CF: 0.03%-
1142 0.71%; LWP: 0.02-2.89 g m⁻²) to those of WRF-Chem_ARI. *This may be explained as*
1143 *the different parameterization treatments of cloud droplet number concentration*
1144 *(CDNC) simulated by the three coupled models with/without enabling ACI effects. The*
1145 *cloud condensation nuclei activated from aerosol particles can increase CDNC and*
1146 *impact on LWP and CF. Without enabling any aerosol feedbacks or only enabling ARI,*
1147 *the CDNC is default prescribed as a constant value of 250 cm⁻³ in the Morrison scheme*
1148 *of WRF-CMAQ and WRF-Chem and 300 cm⁻³ in the Thompson scheme of WRF-*
1149 *CHIMERE. When only ACI or both ARI and ACI are enabled, the online calculating of*
1150 *prognostic CDNC is performed in WRF-Chem and WRF-CHIMERE by using the*
1151 *method of maximum supersaturation (Abdul-Razzak and Ghan, 2002; Chapman et al.,*
1152 *2009; Tuccella et al., 2019). Although we have obtained preliminary quantitative results*
1153 *of the ACI effects on regional precipitation, CF, and LWP, it should be kept in mind that*

Deleted: Figure

Deleted: S11

Deleted: .

Deleted: Figure

Deleted: S12

Deleted:

Deleted: Figure

Deleted: S13

Deleted:

1163 several limitations in representing ACI effects still exist in state-of-the-art two-way
 1164 coupled models; these include a lack of consideration of the responses of convective
 1165 clouds to ACI (Tuccella et al., 2019), and a lack of numerical descriptions of giant cloud
 1166 condensation nuclei (Wang et al., 2021) and heterogeneous ice nuclei (Keita et al.,
 1167 2020).

1168
 1169 Table 3. Statistical metrics (R, MB, NMB, NGE, and RMSE) between annual
 1170 simulations and satellite retrievals of surface shortwave and longwave radiation, TOA
 1171 shortwave and longwave radiation, precipitation, cloud fraction, and liquid water path
 1172 in eastern China. The best results are in bold, while mean simulations and observations
 1173 are in italics.

Variables	Statistics	WRF-CMAQ_NO	WRF-CMAQ_ARI	WRF-Chem_NO	WRF-Chem_ARI	WRF-Chem_BOTH	WRF-CHIMERE_NO	WRF-CHIMERE_ARI	WRF-CHIMERE_BOTH
Surface shortwave radiation (172.74 W m ⁻²)	Mean_sim	<i>197.15</i>	<i>180.94</i>	<i>203.48</i>	<i>194.52</i>	<i>201.45</i>	<i>197.39</i>	<i>191.34</i>	<i>195.58</i>
	R	0.76	0.75	0.73	0.78	0.75	0.61	0.64	0.66
	MB	24.41	8.21	30.74	21.78	28.71	24.75	18.71	32.94
	NMB (%)	14.13	4.75	17.79	12.61	16.62	14.34	10.84	13.29
	<u>NGE (%)</u>	15.13	8.66	18.61	13.53	17.38	17.44	14.42	15.83
	RMSE	30.25	20.37	35.34	26.88	32.80	34.70	29.60	31.45
Surface longwave radiation (322.3 W m ⁻²)	Mean_sim	<i>316.25</i>	<i>315.83</i>	<i>312.96</i>	<i>312.60</i>	<i>312.32</i>	<i>313.33</i>	<i>314.60</i>	<i>314.47</i>
	R	0.98	0.98	0.98	0.98	0.98	0.99	0.99	0.99
	MB	-6.05	-6.46	-9.34	-9.70	-9.97	-9.66	-8.39	-8.53
	NMB (%)	-1.88	-2.00	-2.90	-3.01	-3.09	-2.99	-2.60	-2.64
	<u>NGE (%)</u>	3.22	3.46	3.70	3.77	3.84	3.96	3.60	3.69
	RMSE	13.65	14.13	14.81	14.97	15.17	15.47	14.52	14.72
TOA shortwave radiation (111.56 W m ⁻²)	Mean_sim	<i>107.76</i>	<i>112.68</i>	<i>110.38</i>	<i>110.95</i>	<i>107.16</i>	<i>114.33</i>	<i>116.62</i>	<i>113.00</i>
	R	0.81	0.79	0.69	0.68	0.62	0.65	0.65	0.65
	MB	-3.80	1.13	-1.18	-0.61	-4.40	3.12	5.42	1.89
	NMB (%)	-3.40	1.01	-1.05	-0.55	-3.94	2.81	4.87	3.70
	<u>NGE (%)</u>	10.19	10.45	11.52	10.96	11.69	14.43	14.36	12.93
	RMSE	15.75	16.04	17.07	16.10	17.21	20.85	20.67	18.96
TOA longwave radiation (233.68 W m ⁻²)	Mean_sim	<i>231.54</i>	<i>232.26</i>	<i>234.34</i>	<i>233.96</i>	<i>234.39</i>	<i>232.52</i>	<i>232.17</i>	<i>233.18</i>
	R	0.88	0.90	0.91	0.91	0.92	0.74	0.74	0.76
	MB	-2.14	-1.42	0.66	0.28	0.71	-0.61	-0.96	0.05
	NMB (%)	-0.92	-0.61	0.28	0.12	0.30	-0.26	-0.41	0.02
	<u>NGE (%)</u>	2.28	2.04	1.79	1.79	1.74	3.02	2.98	2.92
	RMSE	6.94	6.20	6.00	5.94	5.86	10.10	10.07	9.70
Precipitation (948.91 mm y ⁻¹)	Mean_sim	<i>872.42</i>	<i>896.98</i>	<i>1069.06</i>	<i>1056.95</i>	<i>1081.84</i>	<i>1165.06</i>	<i>1160.35</i>	<i>1163.7</i>
	R	0.71	0.71	0.71	0.71	0.70	0.69	0.69	0.69
	MB	-76.49	-51.93	120.15	108.04	132.94	207.05	202.35	205.76
	NMB (%)	-9.23	-8.40	12.66	11.39	14.01	21.61	21.12	21.48
	<u>NGE (%)</u>	32.46	34.36	44.54	43.38	45.13	42.54	42.52	42.58
	RMSE	573.14	595.76	675.91	668.92	693.74	776.60	786.36	790.73
Cloud cover (64.09 %)	Mean_sim	<i>52.51</i>	<i>53.32</i>	<i>48.18</i>	<i>47.80</i>	<i>47.46</i>	<i>58.12</i>	<i>57.98</i>	<i>58.35</i>
	R	0.68	0.68	0.69	0.69	0.68	0.66	0.66	0.64

197 models. *The evaluations between surface measurements and simulations of PM_{2.5} and*
198 *O₃ are presented below, and the performance assessments of other gaseous pollutants*
199 *are in Section 2 of Supplement.*

1200 The R values of annual PM_{2.5} concentrations for WRF-CMAQ (0.68) were the
1201 highest, followed by WRF-Chem (0.65–0.68), and WRF-CHIMERE (0.52–0.53). All
1202 three models showed higher correlations in winter compared with those in other seasons
1203 (Fig. 7). *As shown in Table 4 and Figs. 6–7, WRF-CMAQ underestimated annual and*
1204 *seasonal (except for autumn) PM_{2.5} concentrations with NMBs ranging from –9.78%*
1205 *to –6.39% and –17.68% to +5.17%, respectively. WRF-Chem generated both*
1206 *overestimations and underestimations of PM_{2.5} at the annual and seasonal scales, with*
1207 *related NMBs varying from –39.11% to +24.72%, respectively.* Meanwhile, WRF-
1208 CHIMERE excessively overestimated annual and seasonal PM_{2.5} concentrations (NMB:
1209 +19.51% to +75.47%). *These biases could be related to different aerosol and gas phase*
1210 *mechanisms, dust and sea salt emission schemes, chemical ICs and BCs, and aerosol*
1211 *size distribution treatments applied in the three two-way coupled models.* Based on the
1212 differences in NMBs between simulations with ARI and those with no aerosol
1213 feedbacks, ARI-induced annual and seasonal NMB variations of WRF-CMAQ_ARI
1214 and WRF-Chem_ARI ranged from +3.01% to +4.21% and +3.07% to +5.02%,
1215 respectively, indicating that the enabling of ARI feedbacks slightly reduced annual and
1216 seasonal (except for autumn) underestimations of PM_{2.5} concentrations. Note that
1217 WRF-CHIMERE_ARI further overestimated the annual and seasonal PM_{2.5}, with an
1218 increase in NMB of up to 10.04%. The increases in PM_{2.5} concentrations caused by ARI
1219 effects can be attributed to synergetic decreases in SSR, T2, WS10, and PBLH, and
1220 increases in RH2. With ACI feedbacks further enabled, WRF-Chem_BOTH largely
1221 underestimated the annual and seasonal PM_{2.5}, with NMBs varying from –24.15% to
1222 –14.44% compared with WRF-Chem_ARI. WRF-CHIMERE_BOTH tended to
1223 decrease (–2.1% to –0.51%) annual and autumn–winter NMBs, and increase (+0.35%
1224 to +3.04%) spring–summer NMBs. Further comparison between ARI- and ACI-
1225 induced NMB variations demonstrates the key point that ARI-induced variations in
1226 PM_{2.5} concentrations were smaller than those induced by ACI in WRF-Chem, but this
1227 pattern was reversed in WRF-CHIMERE. This may be explained by WRF-CHIMERE
1228 incorporating the process of dust aerosols serving as IN, which was not included in
1229 WRF-Chem in this study.

1230 *For O₃, WRF-CHIMERE (R = 0.62) exhibited the highest correlation, followed by*
1231 *WRF-CMAQ (R = 0.55), and WRF-Chem (R = 0.45) (Table 4 and Fig. S16).* WRF-
1232 CMAQ slightly underestimated annual O₃, with NMBs and NGEs of –12.57% to
1233 –11.52%, *but*, WRF-Chem and WRF-CHIMERE both significantly overestimated it,
1234 with NMBs of 47.82%–48.10% and 29.46%–29.75%, respectively. The seasonal results
1235 of statistical metrics showed patterns that were consistent with annual simulations, and
1236 summer O₃ pollution levels were better simulated than those in other seasons (Fig. 6).
1237 *All models with ARI feedbacks enabled resulted in slight decreases in annual and*
1238 *seasonal O₃ NMBs and NGEs, ranging from –3.02% to +0.85% (the only positive value*
1239 *of +0.85% was produced by WRF-CMAQ in summer) and from –1.42% to –0.75%,*
1240 *respectively.* Meanwhile, for ACI effects, WRF-Chem and WRF-CHIMERE had

Formatted: Font: Italic

Formatted: Font: Italic

Deleted: Figure

Formatted: Font: Italic, Font color: Blue

Formatted: Font: Italic

Formatted: Font: Italic, Font color: Blue

Deleted: These biases were produced by the configurations of different aerosol and gas phase mechanisms, online dust emission schemes, and chemical ICs and BCs in the two-way coupled models....

Deleted: best

Deleted: model performance

Formatted: Font: Italic, Font color: Blue

Deleted: Figure

Deleted: S15

Deleted: 7.83

Deleted: , but

Deleted: Figure

Formatted: Font: Italic, Font color: Blue

253 *increased annual O₃ NMBs and NGEs of 0.12%, 0.65% and 0.40%–0.55%,*
 254 *respectively.* ACI-induced seasonal NMB variations were different for WRF-Chem
 255 compared with WRF-CHIMERE; WRF-Chem increased in spring–summer and
 256 decreased in autumn–winter, while WRF-CHIMERE increased in all seasons except for
 257 winter (Fig. 7). *Such diversity in NMB and NGE variations can be explained by two*
 258 *aspect differences. For model-top boundary conditions, the WRF-CMAQ and WRF-*
 259 *Chem models employed the parameterization scheme of O₃-potential vorticity and*
 260 *WRF-CHIMERE used the climatological data from LMDz-INCA. For gas-phase*
 261 *chemistry mechanisms, three coupled models incorporate a variety of photolytic*
 262 *reactions, with a more comprehensive explanation provided in Section 4.2.*

263 A comprehensive assessment of the effects of seven gas-phase chemical
 264 mechanisms (RADM2, RADMKA, RACM-ESRL, CB05Clx, CB05-TUCL, CBMZ,
 265 and MOZART-4) on O₃ simulations via three two-way coupled models (WRF-Chem,
 266 WRF-CMAQ, and COSMO-ART) was conducted by Knote et al. (2015); they
 267 concluded that the O₃ concentrations simulated via WRF-Chem with the CBMZ
 268 mechanism were closest to the mean values of multiple models over North America and
 269 Europe in spring and summer. However, in contrast to North America and Europe, the
 270 two-way coupled WRF-Chem with CBMZ had the poorest performance during spring
 271 in eastern China. In addition, ARI and/or ACI effects contribute to atmospheric
 272 dynamics and stability (as mentioned in the PBLH evaluation part of Section 1.1 in
 273 Supplement), as well as photochemistry and heterogeneous reactions, and, in turn, they
 274 will eventually influence O₃ formation (Xing et al., 2017; Qu et al., 2021; Zhu et al.,
 275 2021).

277 Table 4. Statistical metrics (R, MB, NMB, NGE, and RMSE) between annual
 278 simulations and observations of surface PM_{2.5}, O₃, NO₂, SO₂, and CO in eastern China.
 279 The best results are in bold, while mean simulations and observations are in italics.

Variables	Statistics	WRF-CMAQ_NO	WRF-CMAQ_ARI	WRF-Chem_NO	WRF-Chem_ARI	WRF-Chem_BOTH	WRF-CHIMERE_NO	WRF-CHIMERE_ARI	WRF-CHIMERE_BOTH
PM _{2.5} (44.99 µg/m ³)	Mean_sim	<i>40.59</i>	<i>42.12</i>	<i>44.45</i>	<i>46.65</i>	<i>38.33</i>	<i>62.17</i>	<i>65.36</i>	<i>65.13</i>
	R	0.68	0.68	0.65	0.65	0.69	0.52	0.53	0.53
	MB	-4.40	-2.87	-0.54	1.66	-6.66	17.18	20.37	20.14
	NMB (%)	-9.78	-6.39	-1.21	3.69	-14.81	38.19	45.27	44.76
	NGE (%)	46.41	47.08	57.82	59.91	52.10	89.85	84.10	41.07
	RMSE	27.62	27.69	32.58	34.64	32.48	55.13	60.25	59.41
O ₃ (62.23 µg/m ³)	Mean_sim	<i>55.06</i>	<i>54.41</i>	<i>88.53</i>	<i>87.81</i>	<i>87.89</i>	<i>76.92</i>	<i>76.48</i>	<i>76.89</i>
	R	0.54	0.55	0.46	0.45	0.45	0.62	0.62	0.62
	MB	-7.17	-7.83	26.30	25.58	25.65	14.69	14.25	14.66
	NMB (%)	-11.52	-12.57	42.26	41.10	41.22	23.60	22.90	23.55
	NGE (%)	41.02	41.40	87.02	86.17	86.57	58.17	57.63	58.18
	RMSE	28.32	28.68	48.10	47.99	47.82	29.65	29.46	29.75
NO ₂ (31.2 µg/m ³)	Mean_sim	<i>33.94</i>	<i>34.46</i>	<i>21.17</i>	<i>21.98</i>	<i>21.40</i>	<i>21.85</i>	<i>22.20</i>	<i>22.24</i>
	R	0.59	0.60	0.50	0.50	0.50	0.55	0.56	0.56
	MB	2.74	3.26	-10.03	-9.22	-9.80	-9.35	-9.00	-8.96
	NMB (%)	8.77	10.44	-32.14	-29.55	-31.40	-29.96	-28.84	-28.78

Deleted: of...+...12% ...and +...65% and 0.40%–0.55%,
 respectively. ACI-induced seasonal NMB variations were
 different for WRF-Chem compared with WRF-CHIMERE;
 WRF-Chem increased in spring–summer and decreased in
 autumn–winter, while WRF-CHIMERE increased in all
 seasons except for winter (Figure ...ig. 6

Deleted: Such diversity in NMB variation can be explained
 by configuration differences in gas-phase chemistry
 mechanisms, which involve various photolytic reactions (a
 more detailed explanation can be found in Section 4.2).

Formatted: Font: (Asian) 等线, Font color: Blue,
 Ligatures: Standard + Contextual

Deleted: Section 3.1

Deleted: According to the annual statistical results (Table 4
 and Figure S16), the NO₂ simulated by all three models had
 comparable correlations (0.50–0.60) with ground-based
 observations. WRF-CMAQ slightly overestimated NO₂
 (MBs of +2.74 to +3.26 µg m⁻³, and NMBs of +8.77% to
 +10.44%), but WRF-Chem (MBs of -10.03 to -9.22 µg
 m⁻³, and NMBs of -32.14% to -29.55%) and WRF-
 CHIMERE (MBs of -9.35 to -8.96 µg m⁻³, and NMBs of
 -29.96% to -28.73%) tended to largely underestimate NO₂
 in eastern China. For seasonal variations (Figure 6), WRF-
 CMAQ had the best performance in winter, and generally
 overestimated NO₂ in all seasons (NMBs of -2.21% to
 34.34%). Both WRF-Chem and WRF-CHIMERE had

Deleted: For CO (Table 4), WRF-CHIMERE (0.47–0.48

Formatted: Font: Italic, Font color: Blue

Formatted

Formatted

Formatted

Formatted

Formatted

Formatted

Formatted: Font: Italic, Font color: Blue

Formatted

Formatted

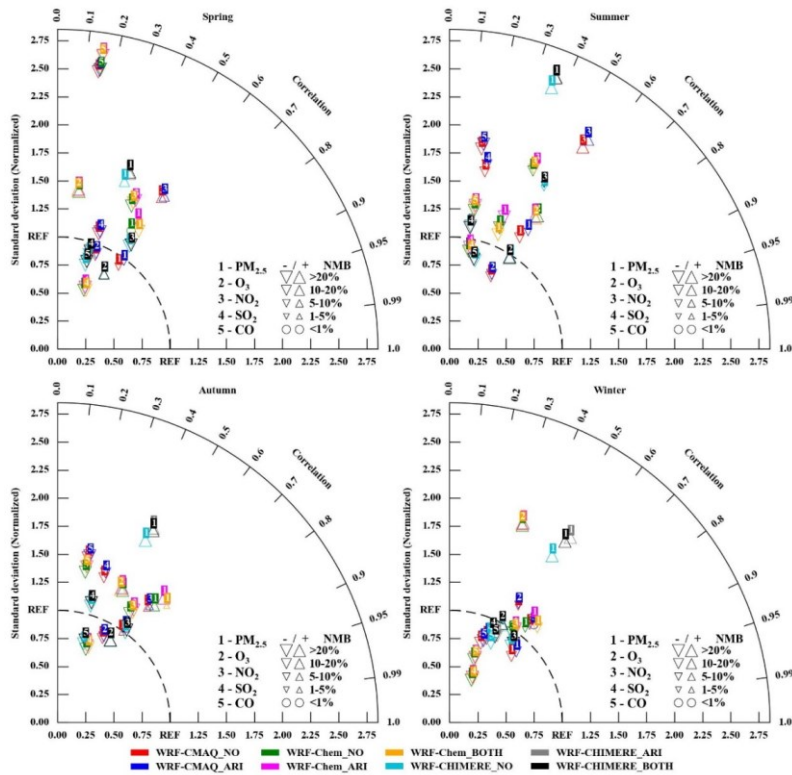
Formatted

Formatted

Formatted

Formatted

Formatted



Deleted: 6

Deleted: Figure

Deleted: 7

Deleted:

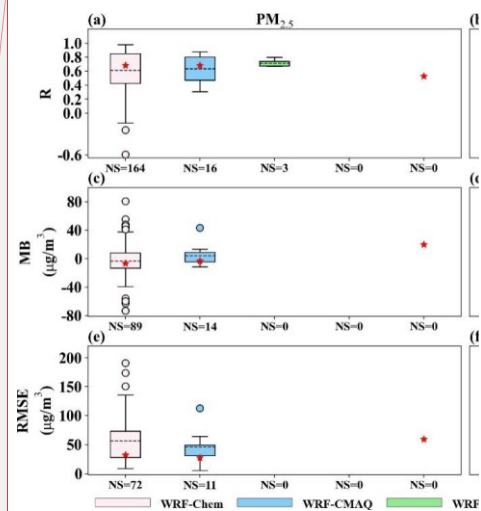


Figure 7. Comparisons of model capacities between our study (red stars) and previous literature (box plots) in terms of surface $PM_{2.5}$ and O_3 concentrations in eastern China. Note that red stars in the fifth column of each subgraph represent the statistical metrics of WRF-CHIMERE in this study.

1477

1478

1479

1480

1481

1482

1483

1484

1485

1486

1487

1488

1489

1490

Figure 7. Taylor diagrams (R, normalized standard deviation, and NMB) of seasonal $PM_{2.5}$, O_3 , NO_2 , SO_2 , and CO via three two-way coupled models (WRF-CMAQ, WRF-Chem, and WRF-CHIMERE) with/without ARI and/or ACI effects in eastern China compared with surface observations.

In a similar manner to the meteorological variables presented above, we aimed to conduct quality assurance for the statistical metrics by making further comparisons with $PM_{2.5}$ and O_3 results from previous model evaluations (summarized in Fig. S20). The performances of WRF-CMAQ and WRF-Chem in simulating $PM_{2.5}$ in this study were better than the average levels of previous studies from eastern China. For O_3 , WRF-Chem simulations performed worse than the average level of previous studies. Although the R values of O_3 simulated by WRF-CMAQ in this study were lower than the average level of previous studies, the RMSEs in this study were smaller.

4.2 Satellite-borne observations

1491

1492

1493

1494

1495

1496

In this section, we further investigate the discrepancies among different models in terms of the calculated AOD and column concentrations of gases (O_3 , NO_2 , SO_2 , CO, and NH_3), and compare them with various satellite observations. For NH_3 , owing to not setting the output of simulated NH_3 concentrations in WRF-CHIMERE, the discussion here only includes the results from WRF-CMAQ and WRF-Chem.

As shown in Table 5, annual AOD at 550 nm, TCO, NO_2 , and CO simulated by all

1508 three models agreed most closely with satellite observations, with correlation
 1509 coefficients of 0.80–0.98; these were followed by NH₃ (0.75–0.76), and SO₂ (0.50–
 1510 0.53). WRF-CMAQ presented negative biases for annual AOD (–0.01), TCO (–5.92
 1511 Dobson Units (DU)), SO₂ (–0.03 to –0.02 DU), CO (–1.25 × 10¹⁷ molecules cm^{–2}), and
 1512 NH₃ (–2.95 × 10¹⁵ molecules cm^{–2}), but a positive bias for NO₂ (1.09–1.21
 1513 petamolecules cm^{–2}). For AOD, WRF-Chem and WRF-CHIMERE produced positive
 1514 and negative MBs of +0.09 and –0.06, respectively. Both WRF-Chem and WRF-
 1515 CHIMERE overestimated NO₂ (0.28–0.63 petamolecules cm^{–2}) and CO (0.93–1.21 ×
 1516 10¹⁷ molecules cm^{–2}), and underestimated O₃ (–10.99 to –3.63 DU) and SO₂ (–0.03 to –
 1517 0.02 DU). Similar to WRF-CMAQ, WRF-Chem also underestimated NH₃ by
 1518 approximately –3.14 × 10¹⁵ molecules cm^{–2}.

1519 For seasonal variations, relatively high correlation relationships (0.71–0.88) of
 1520 AOD were present in autumn, with lower values (0.53–0.84) in other seasons (Fig. 8).
 1521 WRF-CMAQ and WRF-Chem tended to underestimate AOD in summer (MBs of –0.1
 1522 to –0.4) and overestimate it in other seasons (MBs of 0.01–0.05). WRF-CHIMERE had
 1523 positive biases (0.03–0.04) in winter and negative biases (–0.10 to –0.01) in other
 1524 seasons. For TCO (Fig. S24), the model performances of WRF-CMAQ and WRF-Chem
 1525 in spring and winter were slightly better than those in summer and autumn, but all
 1526 seasonal R values were greater than 0.89. Both WRF-CMAQ (–9.53 to –0.72 DU) and
 1527 WRF-Chem (–24.62 to +10.57 DU) had negative biases in all seasons (note: WRF-
 1528 Chem except for autumn). WRF-CHIMERE was better at capturing TCO in spring and
 1529 summer (overestimations of +9.19 to +29.20 DU) than in autumn and winter
 1530 (underestimations of –33.75 to –19.40 DU). The R values of NO₂ columns for all three
 1531 models were slightly higher in autumn and winter (0.82–0.91) than in spring and
 1532 summer (0.76–0.84). *The seasonal NO₂ columns were generally underestimated in*
 1533 *WRF-CMAQ (–0.68 to –0.16 DU), WRF-Chem (–1.40 to –0.44 DU), WRF-CHIMERE (–*
 1534 *1.31 to –0.19 DU) (Fig. S22). All models overestimated SO₂ column concentrations in*
 1535 *winter (by approximately 0.01–0.03 DU) but underestimated them in other seasons*
 1536 *(–0.05 to –0.001 DU) (Fig. S23). For NH₃, the only primary alkaline gas in the*
 1537 *atmosphere, better model performances of WRF-CMAQ and WRF-Chem occurred in*
 1538 *summer (R: 0.81–0.87; MB: –3.42 to 2.07 × 10¹⁵ molecules cm^{–2}) (Fig. S25). Ammonia*
 1539 *emissions from fertilizer and livestock have been substantially underestimated in China*
 1540 *(Zhang et al., 2017), and peak values occur in spring and summer (Huang et al., 2012).*
 1541 *In addition, bidirectional exchanges of fertilizer-induced NH₃ were not considered in*
 1542 *our simulations. Compared to above column variables, WRF-CMAQ, WRF-Chem, and*
 1543 *WRF-CHIMERE showed relatively poor performances (R: 0.68–0.79) in simulating*
 1544 *CO columns during spring, summer, and autumn, respectively, compared with other*
 1545 *seasons (Fig. S24). WRF-CMAQ and WRF-CHIMERE respectively underestimated*
 1546 *and overestimated CO columns in other seasons except for summer and spring, with*
 1547 *MBs of –3.29 to 0.31 × 10¹⁷ and –0.62 to 2.09 × 10¹⁷ molecules cm^{–2}, respectively.*
 1548 *WRF-Chem had positive MBs in summer and autumn (4.03–5.12 × 10¹⁷ molecules*
 1549 *cm^{–2}) and negative MBs in spring and winter (–3.15 to –2.10 × 10¹⁷ molecules cm^{–2}).*

1550 Moreover, after comparing the performance results for each pollutant between
 1551 sections 4.1 and 4.2, the only disparity found between evaluations with ground-based

Deleted: Figure

Deleted: 9

Deleted:

Deleted: Figure

Deleted: S19

Deleted:

Deleted: *simulation accuracies of*

Deleted: *via WRF-CHIMERE were significantly better than those using WRF-CMAQ or WRF-Chem in all seasons except for winter*

Formatted: Font: Italic, Font color: Blue

Deleted: *Figure*

Deleted: S20

Deleted: Figure

Deleted: S21

Deleted:

Deleted: Figure

Deleted: S22

Deleted:

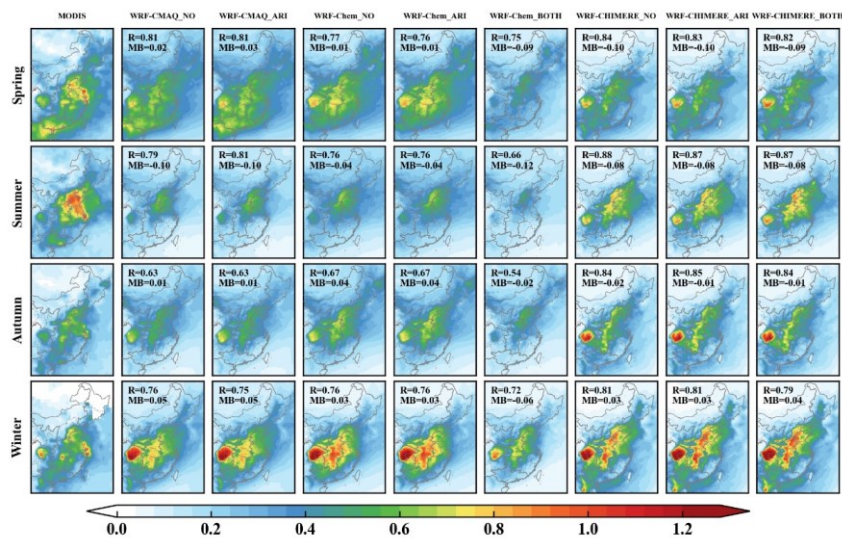
Deleted: Figure

Deleted: S23

O ₃	Mean_sim	306.15	306.15	300.77	300.73	300.46	307.69	307.47	307.75	
VCDs (312.07 DU)	R	0.98	0.98	0.97	0.97	0.97	0.65	0.65	0.65	
	MB	-5.92	-5.92	-10.68	-10.72	-10.99	-3.69	-3.91	-3.63	
	NMB (%)	-1.90	-1.90	-3.43	-3.44	-3.53	-1.19	-1.26	-1.17	
	<i>NGE (%)</i>	2.46	2.46	25.02	25.02	25.08	10.95	10.89	10.93	Formatted: Font: Italic, Font color: Blue
	RMSE	8.91	8.91	83.72	83.73	83.94	39.88	39.71	39.73	Formatted
Tropospheric NO ₂ VCDs (2.71×10 ¹⁵ molecules cm ⁻²)	Mean_sim	3.80	3.91	3.07	3.08	3.06	2.62	2.63	2.63	Formatted
	R	0.85	0.85	0.87	0.87	0.87	0.87	0.87	0.87	Formatted
	MB	1.09	1.21	0.62	0.63	0.61	0.28	0.29	0.29	Formatted
	NMB (%)	40.35	44.64	25.27	25.52	24.89	12.03	12.47	12.42	Formatted
	<i>NGE (%)</i>	52.80	55.08	16.01	16.05	15.17	16.06	16.31	16.24	Formatted
	RMSE	3.18	3.33	2.27	2.27	2.27	1.65	1.67	1.68	Formatted
PBL SO ₂ VCDs (0.09 DU)	Mean_sim	0.07	0.07	0.09	0.09	0.06	0.06	0.06	0.06	Formatted: Font: Italic, Font color: Blue
	R	0.53	0.53	0.56	0.56	0.54	0.50	0.50	0.50	Formatted
	MB	-0.03	-0.02	-0.03	-0.02	-0.03	-0.03	-0.02	-0.02	Formatted
	NMB (%)	-27.32	-25.48	-32.50	-21.50	-35.08	-28.64	-27.31	-27.51	Formatted
	<i>NGE (%)</i>	57.45	58.26	67.55	68.07	64.83	68.31	68.61	68.90	Formatted
	RMSE	0.07	0.07	0.08	0.08	0.07	0.07	0.07	0.07	Formatted
Total CO VCDs (21.60×10 ¹⁷ molecules cm ⁻²)	Mean_sim	20.34	20.35	22.20	22.20	22.21	22.34	22.36	22.33	Formatted
	R	0.83	0.83	0.87	0.87	0.87	0.86	0.86	0.86	Formatted
	MB	-1.26	-1.24	0.93	0.93	0.94	1.19	1.21	1.19	Formatted
	NMB (%)	-5.83	-5.75	4.35	4.37	4.44	5.64	5.70	5.65	Formatted: Font: Italic, Font color: Blue
	<i>NGE (%)</i>	9.33	9.31	10.30	10.28	10.32	11.02	11.06	11.00	Formatted
	RMSE	2.54	2.54	2.69	2.68	2.69	2.57	2.58	2.58	Formatted
Total NH ₃ VCDs (16.05×10 ¹⁵ molecules cm ⁻²)	Mean_sim	13.06	13.15	12.31	12.27	8.63	NA	NA	NA	Formatted
	R	0.76	0.76	0.73	0.73	0.76	NA	NA	NA	Formatted
	MB	-3.00	-2.90	-3.27	-3.32	-3.34	NA	NA	NA	Formatted
	NMB (%)	-18.66	-18.08	-21.01	-21.28	-21.41	NA	NA	NA	Formatted
	<i>NGE (%)</i>	47.69	48.09	50.84	50.80	50.99	NA	NA	NA	Formatted
	RMSE	9.26	9.47	9.48	9.46	9.61	NA	NA	NA	Formatted: Font: Italic, Font color: Blue

1613 NA indicates that outputs of NH₃ column concentrations were not extracted from WRF-CHIMERE

1614 with/without aerosol feedback simulations.



1615

1616 Figure 8. Spatial distributions of seasonal AOD between MODIS observations and
 1617 simulations from WRF-CMAQ, WRF-Chem, and WRF-CHIMERE with and without
 1618 aerosol feedbacks in eastern China.

1619

1620 4.3 Computational performance

1621 Table 5 summarizes the comparative results of central processing unit (CPU) time
 1622 consumption for one day simulations via WRF-CMAQ, WRF-Chem, and WRF-
 1623 CHIMERE with and without aerosol feedbacks in 2017. The results show that
 1624 regardless of whether aerosol feedbacks were enabled, the CPU time consumed by
 1625 WRF-CMAQ simulating one-day meteorology and air quality was shortest, followed
 1626 by WRF-CHIMERE, and WRF-Chem. Compared with simulations without aerosol
 1627 feedbacks, the processing time of WRF-CMAQ with ARI enabled increased by 0.22–
 1628 0.34 hours per day, while increases in the running time of WRF-Chem and WRF-
 1629 CHIMERE were not significant (0.02–0.03 hours per day). The CPU time for both
 1630 WRF-Chem and WRF-CHIMERE with both ARI and ACI effects enabled was slightly
 1631 increased, and the increase in CPU time for the former (0.25 hours per day) was larger
 1632 than that for the latter (0.11 hours per day). Compared with WRF-CMAQ and WRF-
 1633 Chem, the CPU time of WRF-CHIMERE showed obvious seasonal differences, with
 1634 the time in winter and spring being significantly longer than that in summer and
 1635 autumn. These differences can be partially explained by the choice of main configurations,
 1636 including model resolution, model version, and parametrization schemes (cloud
 1637 microphysics, PBL, cumulus, surface layer, land surface, gas-phase chemistry, and
 1638 aerosol mechanisms).

1639

640

Table 5. Summary of running time for different coupled models.

Month	WRF-CMAQ (hour)		WRF-Chem (hour)			WRF-CHIMERE (hour)		
	NO	ARI	NO	ARI	BOTH	NO	ARI	BOTH
Jan.	0.37	0.59	0.69	0.71	0.96	0.67	0.70	0.77
Feb.	0.35	0.60	0.68	0.70	0.93	0.64	0.67	0.73
Mar.	0.39	0.65	0.70	0.72	1.00	0.59	0.62	0.72
Apr.	0.37	0.67	0.67	0.69	0.92	0.54	0.57	0.65
May	0.39	0.71	0.61	0.66	0.86	0.52	0.55	0.62
June	0.40	0.74	0.66	0.67	0.95	0.48	0.51	0.63
July	0.36	0.69	0.65	0.67	0.86	0.49	0.50	0.58
Aug.	0.38	0.68	0.66	0.68	0.90	0.49	0.52	0.61
Sept.	0.37	0.63	0.64	0.65	0.89	0.48	0.52	0.63
Oct.	0.38	0.62	0.66	0.68	0.94	0.53	0.56	0.69
Nov.	0.36	0.58	0.68	0.70	0.91	0.64	0.67	0.72
Dec.	0.35	0.57	0.63	0.66	0.87	0.67	0.70	0.74

1641

1642 5 Conclusions

1643 Applications of two-way coupled meteorology and air quality models have been
 1644 performed in eastern China in recent years, but no research focused on the
 1645 comprehensive assessments of multiple coupled models in this region. To the best of our
 1646 knowledge, this is the first time to conduct comprehensive inter-comparisons among the
 1647 open-sourced two-way coupled meteorology and air quality models (WRF-CMAQ,
 1648 WRF-Chem, and WRF-CHIMERE). This study systemically evaluated the hindcast
 1649 simulations for 2017 and explored the impacts of ARI and/or ACI on model and
 1650 computational performances in eastern China.

1651 After detailed comparisons with ground-based and satellite-borne observations, the
 1652 evaluation results showed that three coupled models perform well for meteorology and
 1653 air quality, especially for surface temperature (with R up to 0.97) and $PM_{2.5}$
 1654 concentrations (with R up to 0.68). The effects of aerosol feedbacks on model
 1655 performances varied depending on the two-way coupled models, variables, and time
 1656 scales. There were around 20%–70% increase of computational time when these two-
 1657 way coupled models enabled aerosol feedbacks against simulations without aerosol-
 1658 radiation-cloud interactions. It is noteworthy that all three coupled models could well
 1659 reproduce the spatiotemporal distributions of satellite-retrieved CO column
 1660 concentrations but not for ground-observed CO concentrations.

1661 With inter-comparisons, some uncertainty sources can be ascertained in
 1662 evaluating aerosol feedback effects. As numerous schemes can be combined in
 1663 configurations of different coupled models, here we only evaluated simulations with
 1664 specific settings. Future comparison works with considering more combinations of
 1665 multiple schemes within the same or different coupled models need to be conducted.
 1666 Among the three coupled models, the numerical representations for specific variable in
 1667 same scheme are diverse, e.g., treatments of cloud cover and cloud optical properties
 1668 in the Fast-JX photolysis scheme. More accurate representations of photolysis

Deleted:

Deleted: In this study, we comprehensively evaluated the annual hindcast simulations for 2017 by the two-way coupled WRF-CMAQ, WRF-Chem, and WRF-CHIMERE models with/without aerosol feedbacks and explored the impacts of ARI and/or ACI on model and computational performances in eastern China. All three two-way coupled models effectively reproduced the spatiotemporal distributions of meteorology and air quality, but some variables (SSR and $PM_{2.5}$) in specific regions showed significant discrepancies. Among meteorological variables at the annual scale, T2 and Q2 were better simulated by the three models than SSR, RH2, WS10, PBLH, and PREP. The SSR, RH2, and WS10 were overestimated with MBs around 15.91–42.65 $W m^{-2}$, 2.53–3.55% and 0.42–1.04 $m s^{-1}$, respectively, while T2 and Q2 were underestimated with MBs ranged from -0.57 to -0.18 $g kg^{-1}$ and -2.00 to 0.68 $^{\circ}C$, respectively. For PREP, the WRF-CMAQ's underestimation was 0.5 $mm day^{-1}$, but WRF-Chem and WRF-CHIMERE overestimated PREP about 1 $mm day^{-1}$. The seasonal variations of simulated meteorological variables in eastern China were also well matched with observations. Overall, the MBs of every meteorological variable simulated by the three models in spring and winter were significantly smaller than those in summer and autumn. In terms of air quality, all three models presented generally acceptable performance for annual surface $PM_{2.5}$, O_3 , and NO_2 concentrations, but not for SO_2 and CO. The overall performances of WRF-CMAQ were best, followed by WRF-Chem, and WRF-CHIMERE. The WRF-CMAQ and WRF-Chem simulations had positive biases for NO_2 (2.74–3.26 $\mu g m^{-3}$) and O_3 (25.58–26.30 $\mu g m^{-3}$), but negative biases for other pollutants, while WRF-CHIMERE simulations had positive biases for $PM_{2.5}$ (17.18–20.37 $\mu g m^{-3}$) and O_3 (14.25–14.69 $\mu g m^{-3}$). The seasonal simulations of surface air quality variables showed better correlations of $PM_{2.5}$, NO_2 , SO_2 , and CO in winter, and O_3 in summer than those in other seasons. Further compared with satellite observations, all coupled models well captured radiation, precipitation, cloud fraction, AOD, and column concentrations of O_3 , NO_2 , CO, and NH_3 both at annual and seasonal scales, but not for LWP and SO_2 .

Formatted: Font: Italic, Font color: Blue

Formatted: Font color: Blue

Formatted: Font: Italic, Font color: Blue

Formatted: Indent: Left 0 ch

Commented [g13]: Prather M J. Photolysis rates in correlated overlapping cloud fields: Cloud-J 7.3 c[J]. Geoscientific Model Development, 2015, 8(8): 2587-2595.

Formatted: Font: Italic, Font color: Blue

Formatted: Font: Italic, Font color: Blue

Deleted: Our evaluations showed that the effects of aerosol feedbacks on model performances varied depending on the two-way coupled models, variables, and time scales. *In general, all three two-way coupled models enabling ARI improved the simulation accuracy of annual and seasonal SSR. However, simulation accuracy of SSR was reduced in WRF-Chem and WRF-CHIMERE with only considering ACI, with slightly improved results after enabling both ARI and ACI. Aerosol feedbacks induced various changes of MB for different variables. For example, MBs decreased for SSR from -19.98 W m^{-2} to -9.24 W m^{-2} , T_2 from $-0.20 \text{ }^\circ\text{C}$ to $-0.15 \text{ }^\circ\text{C}$, Q_2 from -0.17 g kg^{-1} to -0.02 g kg^{-1} , $WS10$ from -0.03 m s^{-1} to -0.01 m s^{-1} and $PBLH$ from -25.25 m to -1.93 m . MBs increased for $PM_{2.5}$ from 1.53 to $3.19 \text{ } \mu\text{g m}^{-3}$ and other gaseous pollutants (NO_2 , SO_2 and CO) as well. In addition, there were computational costs (around 20%–70% increase) involved with turning on aerosol-radiation-cloud effects in two-way coupled models.*

Although many progresses in the developments and enhancements of two-way coupled models have been made and these models are widely applied worldwide, several limitations still exist. As comparison studies of offline models' performances affected by various chemical mechanisms were conducted (Kim et al., 2011; Balzarini et al., 2015; Zheng et al., 2015), relevant assessments targeting two-way coupled models are still lacking. Recently, Wu et al. (2018) and Womack et al. (2021) demonstrated that the non-spherical morphology of BC particles could significantly enhance light absorption and the spherical core-shell mixing

Formatted: Font: Italic, Font color: Blue

Formatted: Font: Italic, Font color: Blue

Formatted: Font: Italic, Font color: Blue

Deleted: *The model inputs and outputs in this study for WRF-CMAQ, WRF-Chem and WRF-CHIMERE with/without enabling ARI or/and ACI effects are available upon request. All simulation and observational data of*

Formatted: Default Paragraph Font, Font: 10 pt, Italic, Font color: Blue, (Asian) Chinese (Simplified, Mainland China)

Formatted: Font: Italic, Font color: Blue

1749 *processes should be taken into account to reduce the evaluation uncertainties. In*
1750 *addition, FDDA nudging technique can attenuate the ARI effects during severe air*
1751 *polluted episodes, and optimal nudging coefficients among different regions need to be*
1752 *determined. Last but not least, the actual mechanisms underlying ACI effects are still*
1753 *unclear, and the new advances in the measurements and parameterizations of CCN/IN*
1754 *activations and precipitation need to be timely incorporated in coupled models.*

1756 Code availability

1757 The source codes of the two-way coupled WRF v4.1.1-CMAQ v5.3.1, WRF-
1758 Chem v4.1.1, and WRF v3.7.1-CHIMERE v2020r1 models are obtained from
1759 <https://github.com/USEPA/CMAQ>, <https://github.com/wrf-model/WRF>, and
1760 <https://www.lmd.polytechnique.fr/chimere>, respectively (last access: November 2020).
1761 *The related source codes, configuration information, namelist files and automated run*
1762 *scripts of these three two-way coupled models are archived at Zenodo with the*
1763 *associated DOI: <https://doi.org/10.5281/zenodo.7901682> (Gao et al., 2023a; link:*
1764 *<https://zenodo.org/record/7901682>).*

1766 Data availability

1767 *The meteorological ICs and BCs used for three coupled models can be obtained*
1768 *at <https://doi.org/10.5281/zenodo.7925012> (Gao et al., 2023b; link:*
1769 *<https://zenodo.org/record/7925012>). The Chemical ICs and BCs used for WRF-CMAQ,*
1770 *WRF-Chem and WRF-CHIMERE are available at*
1771 *<https://doi.org/10.5281/zenodo.7932390> (Gao et al., 2023c; link:*
1772 *<https://zenodo.org/record/7932390>), <https://doi.org/10.5281/zenodo.7932936> (Gao et*
1773 *al., 2023d; link: <https://zenodo.org/record/7932936>), and*
1774 *<https://doi.org/10.5281/zenodo.7933641> (Gao et al., 2023e; link:*
1775 *<https://zenodo.org/record/7933641>), respectively. The emission data used for WRF-*
1776 *CMAQ, WRF-Chem and WRF-CHIMERE can be downloaded from*
1777 *<https://doi.org/10.5281/zenodo.7932430> (Gao et al., 2023f; link:*
1778 *<https://zenodo.org/record/7932430>), <https://doi.org/10.5281/zenodo.7932734> (Gao et*
1779 *al., 2023g; link: <https://zenodo.org/record/7932734>), and*
1780 *<https://doi.org/10.5281/zenodo.7931614> (Gao et al., 2023h; link:*
1781 *<https://zenodo.org/record/7931614>), respectively. The DOIs and links regarding the*
1782 *output data of each simulation scenario are presented in Table S9. All data used to*
1783 *create figures and tables in this study are provided in an open repository on Zenodo*
1784 *(<https://doi.org/10.5281/zenodo.7750907>, Gao et al., 2023i; link:*
1785 *<https://zenodo.org/record/7750907>).*

1787 Author contributions

1788 CG, ZX, AX performed the majority of the source code configuration of WRF-
1789 CMAQ, WRF-Chem and WRF-CHIMERE, designed the numerical simulations to
1790 carry them out, related analysis, figure plotting, and paper writing. QT, HZ, SZ, GY,
1791 MZ and XS were involved with the original research plan and made suggestions for the

1883 paper writing.

1884

1885 Competing interests

1886 The contact author has declared that neither they nor their co-authors have any
1887 competing interests.

1888

1889 Acknowledgements

1890 The authors are very grateful to David Wong, Chun Zhao and Laurent Menut who
1891 provided detailed information on the two-way coupled WRF-CMAQ, WRF-Chem and
1892 WRF-CHIMERE models, respectively.

1893

1894 Financial support

1895 This study was financially sponsored by the Youth Innovation Promotion
1896 Association of Chinese Academy of Sciences, China (grant nos. 2022230), the National
1897 Key Research and Development Program of China (grant nos. 2017YFC0212304 &
1898 2019YFE0194500), the Talent Program of Chinese Academy of Sciences
1899 (Y8H1021001), and the National Natural Science Foundation of China (grant nos.
1900 42171142 & 41771071).

1901

1902 References

1903 *Abdul-Razzak, H. and Ghan, S. J.: A parameterization of aerosol activation 3. Sectional*
1904 *representation, J. Geophys. Res. Atmos., 107, AAC-1, <https://doi.org/10.1029/2001JD000483>,*
1905 *2002.*

1906 Alapaty, K., Herwehe, J. A., Otte, T. L., Nolte, C. G., Bullock, O. R., Mallard, M. S., Kain, J. S.,
1907 and Dudhia, J.: Introducing subgrid-scale cloud feedbacks to radiation for regional
1908 meteorological and climate modeling, *Geophys. Res. Lett.*, 39, 1–5,
1909 <https://doi.org/10.1029/2012GL054031>, 2012.

1910 *Archer-Nicholls, S., Lowe, D., Utembe, S., Allan, J., Zaveri, R. A., Fast, J. D., Hodnebrog, Ø.,*
1911 *Denier Van Der Gon, H., and Mcfiggans, G.: Gaseous chemistry and aerosol mechanism*
1912 *developments for version 3.5.1 of the online regional model, WRF-Chem, Geosci. Model Dev.,*
1913 *7, 2557–2579, <https://doi.org/10.5194/gmd-7-2557-2014>, 2014.*

1914 Baklanov, A., Schlünzen, K., Suppan, P., Baldasano, J., Brunner, D., Aksoyoglu, S., Carmichael,
1915 G., Douros, J., Flemming, J., and Forkel, R.: Online coupled regional meteorology chemistry
1916 models in Europe: current status and prospects, *Atmos. Chem. Phys.*, 14, 317–398,
1917 <https://doi.org/10.5194/acp-14-317-2014>, 2014.

1918 *Balzarini Briant, R., Tuccella, P., Deroubaix, A., Khvorostyanov, D., Menut, L., Mailler, S., and*
1919 *Turquety, S.: Aerosol-radiation interaction modelling using online coupling between the WRF*
1920 *3.7.1 meteorological model and the CHIMERE 2016 chemistry-transport model, through the*
1921 *OASIS3-MCT coupler, Geosci. Model Dev., 10, 927–944, [https://doi.org/10.5194/gmd-10-](https://doi.org/10.5194/gmd-10-927-2017)
1922 [927-2017](https://doi.org/10.5194/gmd-10-927-2017), 2017.*

1923 *Briant, R., Tuccella, P., Deroubaix, A., Khvorostyanov, D., Menut, L., Mailler, S., and Turquety, S.:*
1924 *Aerosol-radiation interaction modelling using online coupling between the WRF 3.7.1*

Formatted: Font: Italic, Font color: Blue

Formatted: Font: Italic, Font color: Blue

Deleted: Balzarini, A., Pirovano, G., Honzak, L., Žabkar, R., Curci, G., Forkel, R., Hirtl, M., San José, R., Tuccella, P., and Grell, G. A.: WRF-Chem model sensitivity to chemical mechanisms choice in reconstructing aerosol optical properties, *Atmos. Environ.*, 115, 604–619, <https://doi.org/10.1016/j.atmosenv.2014.12.033>, 2015.

Formatted: Font: Italic, Font color: Blue

931 *meteorological model and the CHIMERE 2016 chemistry-transport model, through the*
 932 *OASIS3-MCT coupler, Geosci. Model Dev., 10, 927–944, [https://doi.org/10.5194/gmd-10-](https://doi.org/10.5194/gmd-10-927-2017)*
 933 *927-2017, 2017.*

934 Brunner, D., Savage, N., Jorba, O., Eder, B., Giordano, L., Badia, A., Balzarini, A., Baro, R.,
 935 Bianconi, R., and Chemel, C.: Comparative analysis of meteorological performance of coupled
 936 chemistry-meteorology models in the context of AQMEII phase 2, Atmos. Environ., 115, 470–
 937 498, <https://doi.org/10.1016/j.atmosenv.2014.12.032>, 2015.

938 Campbell, P., Zhang, Y., Wang, K., Leung, R., Fan, J., Zheng, B., Zhang, Q., and He, K.: Evaluation
 939 of a multi-scale WRF-CAM5 simulation during the 2010 East Asian Summer Monsoon, Atmos.
 940 Environ., 169, 204–217, <https://doi.org/10.1016/j.atmosenv.2017.09.008>, 2017.

941 Carslaw, K. S., Boucher, O., Spracklen, D. V., Mann, G. W., Rae, J. G. L., Woodward, S., and
 942 Kulmala, M.: A review of natural aerosol interactions and feedbacks within the Earth system,
 943 Atmos. Chem. Phys., 10, 1701–1737, <https://doi.org/10.5194/acp-10-1701-2010>, 2010.

944 *Chapman, E. G., Jr, W. I. G., Easter, R. C., Barnard, J. C., Ghan, S. J., Pekour, M. S., and Fast, J.*
 945 *D.: and Physics Coupling aerosol-cloud-radiative processes in the WRF-Chem model:*
 946 *Investigating the radiative impact of elevated point sources, 945–964,*
 947 *<https://doi.org/10.5194/acp-9-945-2009>, 2009.*

948 Chen, L., Gao, Y., Zhang, M., Fu, J. S., Zhu, J., Liao, H., Li, J., Huang, K., Ge, B., and Wang, X.:
 949 MICS-Asia III: Multi-model comparison and evaluation of aerosol over East Asia, Atmos.
 950 Chem. Phys., 19, 11911–11937, <https://doi.org/10.5194/acp-19-11911-2019>, 2019.

951 Ding, Q. J., Sun, J., Huang, X., Ding, A., Zou, J., Yang, X., and Fu, C.: Impacts of black carbon on
 952 the formation of advection–radiation fog during a haze pollution episode in eastern China,
 953 Atmos. Chem. Phys., 19, 7759–7774, <https://doi.org/10.5194/acp-19-7759-2019>, 2019.

954 Dionne, J., von Salzen, K., Cole, J., Mahmood, R., Leitch, W. R., Lesins, G., Folkins, I., and Chang,
 955 R. Y.-W.: Modelling the relationship between liquid water content and cloud droplet number
 956 concentration observed in low clouds in the summer Arctic and its radiative effects, Atmos.
 957 Chem. Phys., 20, 29–43, <https://doi.org/10.5194/acp-20-29-2020>, 2020.

958 Fan, J., Wang, Y., Rosenfeld, D., and Liu, X.: Review of aerosol-cloud interactions: Mechanisms,
 959 significance, and challenges, J. Atmos. Sci., 73, 4221–4252, [https://doi.org/10.1175/JAS-D-](https://doi.org/10.1175/JAS-D-16-0037.1)
 960 [16-0037.1](https://doi.org/10.1175/JAS-D-16-0037.1), 2016.

961 Feng, X., Lin, H., Fu, T.-M., Sulprizio, M. P., Zhuang, J., Jacob, D. J., Tian, H., Ma, Y., Zhang, L.,
 962 and Wang, X.: WRF-GC (v2.0): online two-way coupling of WRF (v3.9.1.1) and GEOS-Chem
 963 (v12.7.2) for modeling regional atmospheric chemistry–meteorology interactions, Geosci.
 964 Model Dev., 14, 3741–3768, <https://doi.org/10.5194/gmd-14-3741-2021>, 2021.

965 *Forkel, R., Werhahn, J., Hansen, A. B., McKeen, S., Peckham, S., Grell, G., and Suppan, P.: Effect*
 966 *of aerosol-radiation feedback on regional air quality—A case study with WRF/Chem, Atmos.*
 967 *Environ., 53, 202–211, <https://doi.org/10.1016/j.atmosenv.2011.10.009>.*

968 Gao, C., Zhang, X., Xiu, A., Huang, L., Zhao, H., Wang, K., and Tong, Q.: Spatiotemporal
 969 distribution of biogenic volatile organic compounds emissions in China, Acta Sci.
 970 Circumstantiae, 39, 4140–4151, <https://doi.org/10.13671/j.hjkxxb.2019.0243>, 2019.

971 Gao, C., Xiu, A., Zhang, X., Tong, Q., Zhao, H., Zhang, S., Yang, G., and Zhang, M.: Two-way
 972 coupled meteorology and air quality models in Asia: a systematic review and meta-analysis of
 973 impacts of aerosol feedbacks on meteorology and air quality, Atmos. Chem. Phys., 22, 5265–
 974 5329, <https://doi.org/10.5194/acp-22-5265-2022>, 2022.

Deleted: Brüggemann, M., Xu, R., Tilgner, A., Kwong, K. C., Mutzel, A., Poon, H. Y., Otto, T., Schaefer, T., Poulain, L., and Chan, M. N.: Organosulfates in ambient aerosol: state of knowledge and future research directions on formation, abundance, fate, and importance, Environ. Sci. Technol., 54, 3767–3782, <https://doi.org/10.1021/acs.est.9b06751>, 2020.

Deleted: Cantrell, W., Shaw, R., and Mazzoleni, C.: Final Technical Report for “Laboratory Measurements of Cloud Scavenging of Interstitial Aerosol in a Turbulent Environment”, DE-SC0018931, Michigan Technological Univ., Houghton, MI (United States), 2022.

Formatted: Font: Italic, Font color: Blue

Deleted:

Formatted: Font: Italic, Font color: Blue

Formatted: Font: Italic, Font color: Blue

988 [*Gao, C., Xiu, A., Zhang, X.: Oservational data for sfdda nudging analysis in WRF model over China*](#)
989 [*during 2017, Zenodo \[Data set\], https://doi.org/10.5281/zenodo.6975602, 2022.*](#)

990 [*Gao, C., Xiu, A., Zhang, X., Tong, Q., Zhao, H., Zhang, S., Yang, G., Zhang, M., Xie, S.: Source*](#)
991 [*codes of WRF v4.1.1-CMAQ v5.3.1, WRF-Chem v4.1.1 and WRF v3.7.1-*](#)
992 [*CHIMERE v2020r1, Zenodo \[software\]. https://doi.org/10.5281/zenodo.7901682,*](#)
993 [*2023a.*](#)

994 [*Gao, C., Xiu, A., Zhang, X., Tong, Q., Zhao, H., Zhang, S., Yang, G., Zhang, M., Xie, S.: FNL*](#)
995 [*data used for producing meteorological ICs/BCs of WRF v4.1.1-CMAQ v5.3.1,*](#)
996 [*WRF-Chem v4.1.1 and WRF v3.7.1-CHIMERE v2020r1, Zenodo \[data set\],*](#)
997 [*https://doi.org/10.5281/zenodo.7925012, 2023b.*](#)

998 [*Gao, C., Xiu, A., Zhang, X., Tong, Q., Zhao, H., Zhang, S., Yang, G., Zhang, M., Xie, S.: Chemical*](#)
999 [*initial and boundary conditions for WRF-CMAQ, Zenodo \[data set\],*](#)
2000 [*https://doi.org/10.5281/zenodo.7932390, 2023c.*](#)

2001 [*Gao, C., Xiu, A., Zhang, X., Tong, Q., Zhao, H., Zhang, S., Yang, G., Zhang, M., Xie, S.: Chemical*](#)
2002 [*initial and boundary conditions for WRF-Chem, Zenodo \[data set\],*](#)
2003 [*https://doi.org/10.5281/zenodo.7932936, 2023d.*](#)

2004 [*Gao, C., Xiu, A., Zhang, X., Tong, Q., Zhao, H., Zhang, S., Yang, G., Zhang, M., Xie, S.: Chemical*](#)
2005 [*initial and boundary conditions for WRF-CHIMERE, Zenodo \[data set\],*](#)
2006 [*https://doi.org/10.5281/zenodo.7933641, 2023e.*](#)

2007 [*Chao Gao, Xuelei Zhang, Aijun Xiu, Qingqing Tong, Hongmei Zhao, Shichun Zhang,*](#)
2008 [*Guangyi Yang, Mengduo Zhang, Shengjin Xie: Emission input data for WRF-*](#)
2009 [*CMAQ, Zenodo \[data set\], https://doi.org/10.5281/zenodo.7932430, 2023f.*](#)

2010 [*Gao, C., Xiu, A., Zhang, X., Tong, Q., Zhao, H., Zhang, S., Yang, G., Zhang, M., Xie, S.: Emission*](#)
2011 [*input data for WRF-Chem, Zenodo \[data set\],*](#)
2012 [*https://doi.org/10.5281/zenodo.7932734, 2023g.*](#)

2013 [*Gao, C., Xiu, A., Zhang, X., Tong, Q., Zhao, H., Zhang, S., Yang, G., Zhang, M., Xie, S.: Emission*](#)
2014 [*input data for WRF-CHMIERE, Zenodo \[data set\],*](#)
2015 [*https://doi.org/10.5281/zenodo.7931614, 2023h.*](#)

2016 [*Gao, C., Xiu, A., Zhang, X., Tong, Q., Zhao, H., Zhang, S., Yang, G., Zhang, M., Xie, S.: Data*](#)
2017 [*used to create figures and tables in the GMD manuscript "Inter-comparison of*](#)
2018 [*multiple two-way coupled meteorology and air quality models \(WRF v4.1.1-CMAQ*](#)
2019 [*v5.3.1, WRF-Chem v4.1.1 and WRF v3.7.1-CHIMERE v2020r1\) in eastern China".*](#)
2020 [*Zenodo \[data set\], https://doi.org/10.5281/zenodo.7750907, 2023i.*](#)

2021 [*Gao, J., Woodward, A., Vardoulakis, S., Kovats, S., Wilkinson, P., Li, L., Xu, L., Li, J., Yang, J.,*](#)
2022 [*and Cao, L.: Haze, public health and mitigation measures in China: A review of the current*](#)
2023 [*evidence for further policy response, *Sci. Total Environ.*, 578, 148–157,*](#)
2024 [*https://doi.org/10.1016/j.scitotenv.2016.10.231, 2017.*](#)

2025 [*Gao, M., Han, Z., Liu, Z., Li, M., Xin, J., Tao, Z., Li, J., Kang, J. E., Huang, K., Dong, X., Zhuang,*](#)
2026 [*B., Li, S., Ge, B., Wu, Q., Cheng, Y., Wang, Y., Lee, H. J., Kim, C. H., Fu, J. S., Wang, T.,*](#)
2027 [*Chin, M., Woo, J. H., Zhang, Q., Wang, Z., and Carmichael, G. R.: Air quality and climate*](#)
2028 [*change, Topic 3 of the Model Inter-Comparison Study for Asia Phase III \(MICS-Asia III\)- Part*](#)
2029 [*I: Overview and model evaluation, *Atmos. Chem. Phys.*, 18, 4859–4884,*](#)
2030 [*https://doi.org/10.5194/acp-18-4859-2018, 2018.*](#)

2031 [*Gao, M., Han, Z., Tao, Z., Li, J., Kang, J.-E., Huang, K., Dong, X., Zhuang, B., Li, S., and Ge, B.:*](#)

Deleted:

2033 Air quality and climate change, Topic 3 of the Model Inter-Comparison Study for Asia Phase
 2034 III (MICS-Asia III)–Part 2: aerosol radiative effects and aerosol feedbacks, *Atmos. Chem.*
 2035 *Phys.*, 20, 1147–1161, <https://doi.org/10.5194/acp-20-1147-2020>, 2020.

2036 Gao, Y., Zhang, M., Liu, Z., Wang, L., Wang, P., Xia, X., Tao, M., and Zhu, L.: Modeling the
 2037 feedback between aerosol and meteorological variables in the atmospheric boundary layer
 2038 during a severe fog-haze event over the North China Plain., *Atmos. Chem. Phys.*, 15, 4279–
 2039 4295, <https://doi.org/10.5194/acp-15-4279-2015>, 2015.

2040 Ge, B., Itahashi, S., Sato, K., Xu, D., Wang, J., Fan, F., Tan, Q., Fu, J. S., Wang, X., and Yamaji,
 2041 K.: Model Inter-Comparison Study for Asia (MICS-Asia) phase III: multimodel comparison
 2042 of reactive nitrogen deposition over China, *Atmos. Chem. Phys.*, 20, 10587–10610,
 2043 <https://doi.org/10.5194/acp-20-10587-2020>, 2020.

2044 Geng, G., Zheng, Y., Zhang, Q., Xue, T., Zhao, H., Tong, D., Zheng, B., Li, M., Liu, F., and Hong,
 2045 C.: Drivers of PM_{2.5} air pollution deaths in China 2002–2017, *Nat. Geosci.*, 14, 645–650,
 2046 <https://doi.org/10.1038/s41561-021-00792-3>, 2021.

2047 Gillies, S., Ward, B., and Petersen, A. S.: Rasterio: Geospatial raster I/O for Python programmers,
 2048 URL <https://github.com/mapbox/rasterio>, 2013.

2049 Govardhan, G. R., Nanjundiah, R. S., Satheesh, S. K., Moorthy, K. K., and Takemura, T.: Inter-
 2050 comparison and performance evaluation of chemistry transport models over Indian region,
 2051 *Atmos. Environ.*, 125, 486–504, <https://doi.org/10.1016/j.atmosenv.2015.10.065>, 2016.

2052 Grell, G. and Baklanov, A.: Integrated modeling for forecasting weather and air quality: A call for
 2053 fully coupled approaches, *Atmos. Environ.*, 45, 6845–6851,
 2054 <https://doi.org/10.1016/j.atmosenv.2011.01.017>, 2011.

2055 Grell, G. A., Peckham, S. E., Schmitz, R., McKeen, S. A., Frost, G., Skamarock, W. C., and Eder,
 2056 B.: Fully coupled “online” chemistry within the WRF model, *Atmos. Environ.*, 39, 6957–6975,
 2057 <https://doi.org/10.1016/j.atmosenv.2005.04.027>, 2005.

2058 Guo, J., Li, Y., Cohen, J. B., Li, J., Chen, D., Xu, H., Liu, L., Yin, J., Hu, K., and Zhai, P.: Shift in
 2059 the temporal trend of boundary layer height in China using long-term (1979–2016) radiosonde
 2060 data, *Geophys. Res. Lett.*, 46, 6080–6089, <https://doi.org/10.1029/2019GL082666>, 2019.

2061 He, K., Huo, H., and Zhang, Q.: Urban air pollution in China: current status, characteristics, and
 2062 progress, *Annu. Rev. Environ. Resour.*, 27, 397,
 2063 <https://doi.org/10.1146/annurev.energy.27.122001.083421>, 2002.

2064 Hogrefe, C., Bash, J. O., Pleim, J. E., Schwede, D. B., Gilliam, R. C., Foley, K. M., Appel, K. W.,
 2065 and Mathur, R.: An Analysis of CMAQ Gas Phase Dry Deposition over North America
 2066 Through Grid-Scale and Land-Use Specific Diagnostics in the Context of AQMEII4, *Atmos.*
 2067 *Chem. Phys. Discuss.*, 1–52, <https://doi.org/10.5194/acp-2023-10>, 2023.

2068 Hong, C., Zhang, Q., Zhang, Y., Tang, Y., Tong, D., and He, K.: Multi-year downscaling application
 2069 of two-way coupled WRF v3.4 and CMAQ v5.0.2 over east Asia for regional climate and air
 2070 quality modeling: model evaluation and aerosol direct effects., *Geosci. Model Dev.*, 10, 2447–
 2071 2470, <https://doi.org/10.5194/gmd-10-2447-2017>, 2017.

2072 Huang, D. and Gao, S.: Impact of different reanalysis data on WRF dynamical downscaling over
 2073 China, *Atmos. Res.*, 200, 25–35, <https://doi.org/10.1016/j.atmosres.2017.09.017>, 2018.

2074 *Huang, X., Song, Y., Li, M., Li, J., Huo, O., Cai, X., Zhu, T., Hu, M., and Zhang, H.: A high-*
 2075 *resolution ammonia emission inventory in China, Global Biogeochem. Cycles*, 26,
 2076 <https://doi.org/10.1029/2011GB004161>, 2012.

Deleted: Guo, J., Miao, Y., Zhang, Y., Liu, H., Li, Z., Zhang, W., He, J., Lou, M., Yan, Y., and Bian, L.: The climatology of planetary boundary layer height in China derived from radiosonde and reanalysis data, *Atmos. Chem. Phys.*, 16, 13309–13319, <https://doi.org/10.5194/acp-16-13309-2016>, 2016.

Deleted: He, J., Zhang, Y., Wang, K., Chen, Y., Leung, L. R., Fan, J., Li, M., Zheng, B., Zhang, Q., and Duan, F.: Multi-year application of WRF-CAM5 over East Asia-Part I: Comprehensive evaluation and formation regimes of O₃ and PM_{2.5}, *Atmos. Environ.*, 165, 122–142, <https://doi.org/10.1016/j.atmosenv.2017.06.015>, 2017.

Formatted: Font: Italic, Font color: Blue

2089 *Jacono, M. J., Delamere, J. S., Mlawer, E. J., Shephard, M. W., Clough, S. A., and Collins, W. D.:*
2090 *Radiative forcing by long - lived greenhouse gases: Calculations with the AER radiative*
2091 *transfer models, J. Geophys. Res. Atmos., 113, <https://doi.org/10.1029/2008JD009944>, 2008.*

2092 Im, U., Bianconi, R., Solazzo, E., Kioutsioukis, I., Badia, A., Balzarini, A., Baró, R., Bellasio, R.,
2093 Brunner, D., and Chemel, C.: Evaluation of operational on-line-coupled regional air quality
2094 models over Europe and North America in the context of AQMEII phase 2. Part I: Ozone,
2095 Atmos. Environ., 115, 404–420, <https://doi.org/10.1016/j.atmosenv.2014.09.042>, 2015a.

2096 Im, U., Bianconi, R., Solazzo, E., Kioutsioukis, I., Badia, A., Balzarini, A., Baró, R., Bellasio, R.,
2097 Brunner, D., and Chemel, C.: Evaluation of operational online-coupled regional air quality
2098 models over Europe and North America in the context of AQMEII phase 2. Part II: Particulate
2099 matter, Atmos. Environ., 115, 421–441, <https://doi.org/10.1016/j.atmosenv.2014.08.072>,
2100 2015b.

2101 IPCC: Climate change 2007: Synthesis Report. Contribution of Working Groups I, II and III to the
2102 Fourth Assessment Report of the Intergovernmental Panel on Climate Change, 2007.

2103 IPCC: Climate change 2021: Synthesis Report. Contribution of Working Groups I, II and III to the
2104 Sixth Assessment Report of the Intergovernmental Panel on Climate Change., 2021.

2105 Itahashi, S., Ge, B., Sato, K., Fu, J. S., Wang, X., Yamaji, K., Nagashima, T., Li, J., Kajino, M., and
2106 Liao, H.: MICS-Asia III: overview of model intercomparison and evaluation of acid deposition
2107 over Asia, Atmos. Chem. Phys., 20, 2667–2693, <https://doi.org/10.5194/acp-20-2667-2020>,
2108 2020.

2109 *Jacobson, M. Z.: Developing, coupling, and applying a gas, aerosol, transport, and radiation model*
2110 *to study urban and regional air pollution, 1994.*

2111 *Jacobson, M. Z.: Development and application of a new air pollution modeling system—Part III.*
2112 *Aerosol-phase simulations, Atmos. Environ., 31, 587–608, [https://doi.org/10.1016/S1352-](https://doi.org/10.1016/S1352-2310(96)00201-4)*

2113 [2310\(96\)00201-4](https://doi.org/10.1016/S1352-2310(96)00201-4), 1997.

2114 *Jacobson, M. Z.: Studying the effects of aerosols on vertical photolysis rate coefficient and*
2115 *temperature profiles over an urban airshed, J. Geophys. Res. Atmos., 103, 10593–10604,*
2116 <https://doi.org/10.1029/98jd00287>, 1998.

2117 *Jacobson, M. Z.: GATOR-GCMM: A global-through urban-scale air pollution and weather forecast*
2118 *model: I. Model design and treatment of subgrid soil, vegetation, roads, rooftops, water, sea*
2119 *ice, and snow. J. Geophys. Res. Atmos., 106, 5385–5401,*
2120 <https://doi.org/10.1029/2000JD900560>, 2001.

2121 Jacobson, M. Z.: Analysis of aerosol interactions with numerical techniques for solving coagulation,
2122 nucleation, condensation, dissolution, and reversible chemistry among multiple size
2123 distributions, J. Geophys. Res. Atmos., 107, AAC-2, <https://doi.org/10.1029/2001JD002044>,
2124 2002.

2125 Keita, S. A., Girard, E., Raut, J.-C., Leriche, M., Blanchet, J.-P., Pelon, J., Onishi, T., and Cirisan,
2126 A.: A new parameterization of ice heterogeneous nucleation coupled to aerosol chemistry in
2127 WRF-Chem model version 3.5.1: evaluation through ISDAC measurements, Geosci. Model
2128 Dev., 13, 5737–5755, <https://doi.org/10.5194/gmd-13-5737-2020>, 2020.

2129 Klein, S. A., McCoy, R. B., Morrison, H., Ackerman, A. S., Avramov, A., Boer, G. de, Chen, M.,
2130 Cole, J. N. S., Del Genio, A. D., and Falk, M.: Intercomparison of model simulations of mixed-
2131 phase clouds observed during the ARM Mixed-Phase Arctic Cloud Experiment. I: Single-layer
2132 cloud, Q. J. R. Meteorol. Soc. A J. Atmos. Sci. Appl. Meteorol. Phys. Oceanogr., 135, 979–

Formatted: Font: Italic, Font color: Blue

Deleted:

Formatted: Font: Italic, Font color: Blue

Deleted:

Deleted: Kärcher, B. and Marcolli, C.: Aerosol–cloud interactions: the representation of heterogeneous ice activation in cloud models, Atmos. Chem. Phys., 21, 15213–15220, <https://doi.org/10.5194/acp-21-15213-2021>, 2021.

Deleted:

Kim, Y., Sartelet, K., and Seigneur, C.: Formation of secondary aerosols over Europe: comparison of two gas-phase chemical mechanisms, Atmos. Chem. Phys., 11, 583–598, <https://doi.org/10.5194/acp-11-583-2011>, 2011.

2145 1002, <https://doi.org/10.1002/qj.416>, 2009.

2146 Knote, C., Tuccella, P., Curci, G., Emmons, L., Orlando, J. J., Madronich, S., Baró, R., Jiménez-

2147 Guerrero, P., Luecken, D., and Hogrefe, C.: Influence of the choice of gas-phase mechanism

2148 on predictions of key gaseous pollutants during the AQMEII phase-2 intercomparison, *Atmos.*

2149 *Environ.*, 115, 553–568, <https://doi.org/10.1016/j.atmosenv.2014.11.066>, 2015.

2150 Kong, L., Tang, X., Zhu, J., Wang, Z., Fu, J. S., Wang, X., Itahashi, S., Yamaji, K., Nagashima, T.,

2151 and Lee, H.-J.: Evaluation and uncertainty investigation of the NO₂, CO and NH₃ modeling

2152 over China under the framework of MICS-Asia III, *Atmos. Chem. Phys.*, 20, 181–202,

2153 <https://doi.org/10.5194/acp-20-181-2020>, 2020.

2154 Li, J., Nagashima, T., Kong, L., Ge, B., Yamaji, K., Fu, J. S., Wang, X., Fan, Q., Itahashi, S., and

2155 Hyo-Jung, L.: Model evaluation and intercomparison of surface-level ozone and relevant

2156 species in East Asia in the context of MICS-Asia Phase III–Part 1: Overview, *Atmos. Chem.*

2157 *Phys.*, 19, 12993–13015, <https://doi.org/10.5194/acp-19-12993-2019>, 2019.

2158 Li, M., Liu, H., Geng, G., Hong, C., Liu, F., Song, Y., Tong, D., Zheng, B., Cui, H., and Man, H.:

2159 Anthropogenic emission inventories in China: a review, *Natl. Sci. Rev.*, 4, 834–866,

2160 <https://doi.org/10.1093/nsr/nwx150>, 2017.

2161 Liu, Z., Wang, Y., Hu, B., Lu, K., Tang, G., Ji, D., Yang, X., Gao, W., Xie, Y., and Liu, J.:

2162 Elucidating the quantitative characterization of atmospheric oxidation capacity in Beijing,

2163 China, *Sci. Total Environ.*, 771, 145306, <https://doi.org/10.1016/j.scitotenv.2021.145306>,

2164 2021.

2165 Ma, Y., Jin, Y., Zhang, M., Gong, W., Hong, J., Jin, S., Shi, Y., Zhang, Y., and Liu, B.: Aerosol

2166 optical properties of haze episodes in eastern China based on remote-sensing observations and

2167 WRF-Chem simulations, *Sci. Total Environ.*, 757, 143784,

2168 <https://doi.org/10.1016/j.scitotenv.2020.143784>, 2021.

2169 *Mailler, S., Menut, L., Khvorostyanov, D., Valari, M., Couvidat, F., Siour, G., Turquety, S., Briant,*

2170 *R., Tuccella, P., and Bessagnet, B.: CHIMERE-2017: from urban to hemispheric chemistry-*

2171 *transport modeling, *Geosci. Model Dev.*, 10, 2397–2423, [https://doi.org/10.1016/j.atmosenv.2014.12.003](https://doi.org/10.5194/gmd-10-</i></i></u></p>
<p>2172 <u><i>2397-2017, 2017.</i></u></p>
<p>2173 <u>Makar, P. A., Gong, W., Milbrandt, J., Hogrefe, C., Zhang, Y., Curci, G., Žabkar, R., Im, U.,</u></p>
<p>2174 <u>Balzarini, A., Baró, R., Bianconi, R., Cheung, P., Forkel, R., Gravel, S., Hirtl, M., Honzak, L.,</u></p>
<p>2175 <u>Hou, A., Jiménez-Guerrero, P., Langer, M., Moran, M. D., Pabla, B., Pérez, J. L., Pirovano, G.,</u></p>
<p>2176 <u>San José, R., Tuccella, P., Werhahn, J., Zhang, J., and Galmarini, S.: Feedbacks between air</u></p>
<p>2177 <u>pollution and weather, Part 1: Effects on weather, <i>Atmos. Environ.</i>, 115, 442–469,</u></p>
<p>2178 <u><a href=), 2015a.*

2179 Makar, P. A., Gong, W., Hogrefe, C., Zhang, Y., Curci, G., Žabkar, R., Milbrandt, J., Im, U.,

2180 Balzarini, A., Baró, R., Bianconi, R., Cheung, P., Forkel, R., Gravel, S., Hirtl, M., Honzak, L.,

2181 Hou, A., Jiménez-Guerrero, P., Langer, M., Moran, M. D., Pabla, B., Pérez, J. L., Pirovano, G.,

2182 San José, R., Tuccella, P., Werhahn, J., Zhang, J., and Galmarini, S.: Feedbacks between air

2183 pollution and weather, part 2: Effects on chemistry, *Atmos. Environ.*, 115, 499–526,

2184 <https://doi.org/10.1016/j.atmosenv.2014.10.021>, 2015b.

2185 *Menut, L., Bessagnet, B., Khvorostyanov, D., Beekmann, M., Blond, N., Colette, A., Coll, I., Curci,*

2186 *G., Foret, G., and Hodzic, A.: CHIMERE 2013: a model for regional atmospheric composition*

2187 *modelling, *Geosci. Model Dev.*, 6, 981–1028, <https://doi.org/10.5194/gmd-6-981-2013>,*

2188 *2013.*

2188 Qu, Y., Voulgarakis, A., Wang, T., Kasoar, M., Wells, C., Yuan, C., Varma, S., and Mansfield, L.:

Deleted: Li, D., Xue, L., Wen, L., Wang, X., Chen, T., Mellouki, A., Chen, J., and Wang, W.: Characteristics and sources of nitrous acid in an urban atmosphere of northern China: Results from 1-yr continuous observations, *Atmos. Environ.*, 182, 296–306, <https://doi.org/10.1016/j.atmosenv.2018.03.033>, 2018.

Deleted: Liu, X.-H., Zhang, Y., Cheng, S.-H., Xing, J., Zhang, Q., Streets, D. G., Jang, C., Wang, W.-X., and Hao, J.-M.: Understanding of regional air pollution over China using CMAQ, part I performance evaluation and seasonal variation, *Atmos. Environ.*, 44, 2415–2426, <https://doi.org/10.1016/j.atmosenv.2010.03.035>, 2010.

Liu, Y., Lu, K., Li, X., Dong, H., Tan, Z., Wang, H., Zou, Q., Wu, Y., Zeng, L., and Hu, M.: A comprehensive model test of the HONO sources constrained to field measurements at rural North China Plain, *Environ. Sci. Technol.*, 53, 3517–3525, <https://doi.org/10.1021/acs.est.8b06367>, 2019.

Deleted: López-Romero, J. M., Montávez, J. P., Jerez, S., Lorente-Plazas, R., Palacios-Peña, L., and Jiménez-Guerrero, P.: Precipitation response to aerosol–radiation and aerosol–cloud interactions in regional climate simulations over Europe, *Atmos. Chem. Phys.*, 21, 415–430, <https://doi.org/10.5194/acp-21-415-2021>, 2021.

Formatted: Font: Italic, Font color: Blue

Deleted:

Formatted: Font: Italic, Font color: Blue

Deleted:

2214 A study of the effect of aerosols on surface ozone through meteorology feedbacks over China,
 2215 Atmos. Chem. Phys., 21, 5705–5718, <https://doi.org/10.5194/acp-21-5705-2021>, 2021.

2216 Rosenfeld, D., Andreae, M. O., Asmi, A., Chin, M., de Leeuw, G., Donovan, D. P., Kahn, R., Kinne,
 2217 S., Kivekäs, N., and Kulmala, M.: Global observations of aerosol-cloud-precipitation-climate
 2218 interactions, Rev. Geophys., 52, 750–808, <https://doi.org/10.1002/2013RG000441>, 2014.

2219 Safieddine, S., Boynard, A., Coheur, P.-F., Hurtmans, D., Pfister, G., Quennehen, B., Thomas, J. L.,
 2220 Raut, J.-C., Law, K. S., and Klimont, Z.: Summertime tropospheric ozone assessment over the
 2221 Mediterranean region using the thermal infrared IASI/MetOp sounder and the WRF-Chem
 2222 model, Atmos. Chem. Phys., 14, 10119–10131, <https://doi.org/10.5194/acp-14-10119-2014>,
 2223 2014.

2224 Stein, O., Schultz, M. G., Bouarar, I., Clark, H., Huijnen, V., Gaudel, A., George, M., and Clerbaux,
 2225 C.: On the wintertime low bias of Northern Hemisphere carbon monoxide found in global
 2226 model simulations, Atmos. Chem. Phys., 14, 9295–9316, [https://doi.org/10.5194/acp-14-9295-](https://doi.org/10.5194/acp-14-9295-2014)
 2227 [2014](https://doi.org/10.5194/acp-14-9295-2014), 2014.

2228 Tang, W., Yang, K., Qin, J., Li, X., and Niu, X.: A 16-year dataset (2000–2015) of high-resolution
 2229 (3 h, 10 km) global surface solar radiation, Earth Syst. Sci. Data, 11, 1905–1915,
 2230 <https://doi.org/10.5194/essd-11-1905-2019>, 2019.

2231 Tuccella, P., Menut, L., Briant, R., Deroubaix, A., Khvorostyanov, D., Mailler, S., Siour, G., and
 2232 Turquety, S.: Implementation of aerosol-cloud interaction within WRF-CHIMERE online
 2233 coupled model: Evaluation and investigation of the indirect radiative effect from anthropogenic
 2234 emission reduction on the Benelux Union, Atmosphere (Basel), 10,
 2235 <https://doi.org/10.3390/atmos10010020>, 2019.

2236 Wallace, J. M. and Hobbs, P. V.: Atmospheric science: an introductory survey, Elsevier, 2006.

2237 Wang, K., Zhang, Y., Yahya, K., Wu, S.-Y., and Grell, G.: Implementation and initial application
 2238 of new chemistry-aerosol options in WRF/Chem for simulating secondary organic aerosols and
 2239 aerosol indirect effects for regional air quality, Atmos. Environ., 115, 716–732,
 2240 <https://doi.org/10.1016/j.atmosenv.2014.12.007>, 2015.

2241 Wang, K., Zhang, Y., Zhang, X., Fan, J., Leung, L. R., Zheng, B., Zhang, Q., and He, K.: Fine-scale
 2242 application of WRF-CAM5 during a dust storm episode over East Asia: Sensitivity to grid
 2243 resolutions and aerosol activation parameterizations, Atmos. Environ., 176, 1–20,
 2244 <https://doi.org/10.1016/j.atmosenv.2017.12.014>, 2018.

2245 Wang, K., Zhang, Y., Yu, S., Wong, D. C., Pleim, J., Mathur, R., Kelly, J. T., and Bell, M.: A
 2246 comparative study of two-way and offline coupled WRF v3.4 and CMAQ v5.0.2 over the
 2247 contiguous US: performance evaluation and impacts of chemistry–meteorology feedbacks on
 2248 air quality, Geosci. Model Dev., 14, 7189–7221, <https://doi.org/10.5194/gmd-14-7189-2021>,
 2249 2021.

2250 Wang, K., Gao, C., Wu, K., Liu, K., Wang, H., Dan, M., Ji, X., and Tong, Q.: ISAT v2. 0: an
 2251 integrated tool for nested-domain configurations and model-ready emission inventories for
 2252 WRF-AQM, Geosci. Model Dev., 16, 1961–1973, <https://doi.org/10.5194/gmd-16-1961-2023>,
 2253 2023.

2254 Wang, S. and Hao, J.: Air quality management in China: Issues, challenges, and options, J. Environ.
 2255 Sci., 24, 2–13, [https://doi.org/10.1016/S1001-0742\(11\)60724-9](https://doi.org/10.1016/S1001-0742(11)60724-9), 2012.

2256 Wang, Z., Wang, Z., Li, J., Zheng, H., Yan, P., and Li, J.: Development of a meteorology-chemistry
 2257 two-way coupled numerical model (WRF-NAQPMS) and its application in a severe autumn

Deleted: Ryu, Y. and Min, S.: Improving Wet and Dry Deposition of Aerosols in WRF - Chem: Updates to Below - Cloud Scavenging and Coarse - Particle Dry Deposition, J. Adv. Model. Earth Syst., 14, e2021MS002792, <https://doi.org/10.1029/2021MS002792>, 2022.

Seinfeld, J. H., Bretherton, C., Carslaw, K. S., Coe, H., DeMott, P. J., Dunlea, E. J., Feingold, G., Ghan, S., Guenther, A. B., and Kahn, R.: Improving our fundamental understanding of the role of aerosol–cloud interactions in the climate system, Proc. Natl. Acad. Sci., 113, 5781–5790, <https://doi.org/10.1073/pnas.1514043113>, 2016.

Deleted: Spataro, F., Ianniello, A., Esposito, G., Allegrini, I., Zhu, T., and Hu, M.: Occurrence of atmospheric nitrous acid in the urban area of Beijing (China), Sci. Total Environ., 447, 210–224, <https://doi.org/10.1016/j.scitotenv.2012.12.065>, 2013.

Formatted: Font: Italic, Font color: Blue

Deleted:

2276 haze simulation over the Beijing-Tianjin-Hebei area, China. *Clim. Environ. Res.*, 19, 153–163,
 2277 <https://doi.org/10.3878/j.issn.1006-9585.2014.13231>, 2014.

2278 *Wiedinmyer, C., Akagi, S. K., Yokelson, R. J., Emmons, L. K., Al-Saadi, J. A., Orlando, J. J., and*
 2279 *Soja, A. J.: The Fire INventory from NCAR (FINN): A high resolution global model to estimate*
 2280 *the emissions from open burning. Geosci. Model Dev.*, 4, 625–641,
 2281 <https://doi.org/10.5194/gmd-4-625-2011>, 2011.

2282 *Wong, D. C., Pleim, J., Mathur, R., Binkowski, F., Otte, T., Gilliam, R., Pouliot, G., Xiu, A., Young,*
 2283 *J. O., and Kang, D.: WRF-CMAQ two-way coupled system with aerosol feedback: software*
 2284 *development and preliminary results, Geosci. Model Dev.*, 5, 299–312,
 2285 <https://doi.org/10.5194/gmd-5-299-2012>, 2012.

2286 *Xing, J., Mathur, R., Pleim, J., Hogrefe, C., Wang, J., Gan, C.-M., Sarwar, G., Wong, D. C., and*
 2287 *McKeen, S.: Representing the effects of stratosphere-troposphere exchange on 3-D O₃*
 2288 *distributions in chemistry transport models using a potential vorticity-based parameterization.*
 2289 *Atmos. Chem. Phys.*, 16, 10865–10877, <https://doi.org/10.5194/acp-16-10865-2016>, 2016.

2290 *Xing, J., Wang, J., Mathur, R., Wang, S., Sarwar, G., Pleim, J., Hogrefe, C., Zhang, Y., Jiang, J.,*
 2291 *and Wong, D. C.: Impacts of aerosol direct effects on tropospheric ozone through changes in*
 2292 *atmospheric dynamics and photolysis rates, Atmos. Chem. Phys.*, 17, 9869–9883,
 2293 <https://doi.org/10.5194/acp-17-9869-2017>, 2017.

2294 *Xu, K.-M. and Randall, D. A.: A semiempirical cloudiness parameterization for use in climate*
 2295 *models. J. Atmos. Sci.*, 53, 3084–3102, [https://doi.org/10.1175/1520-](https://doi.org/10.1175/1520-0469(1996)053<3084:ASCPFU>2.0.CO;2)
 2296 [0469\(1996\)053<3084:ASCPFU>2.0.CO;2](https://doi.org/10.1175/1520-0469(1996)053<3084:ASCPFU>2.0.CO;2), 1996.

2297 *Zaveri, R. A., Easter, R. C., Fast, J. D., and Peters, L. K.: Model for simulating aerosol interactions*
 2298 *and chemistry (MOSAIC). J. Geophys. Res. Atmos.*, 113,
 2299 <https://doi.org/10.1029/2007JD008782>, 2008.

2300 *Zhang, X., Wu, Y., Liu, X., Reis, S., Jin, J., Dragosits, U., Van Damme, M., Clarisse, L., Whitburn,*
 2301 *S., and Coheur, P.-F.: Ammonia emissions may be substantially underestimated in China.*
 2302 *Environ. Sci. Technol.*, 51, 12089–12096, <https://doi.org/10.1021/acs.est.7b02171>, 2017.

2303 *Zhang, Y.: Online-coupled meteorology and chemistry models: history, current status, and outlook,*
 2304 *Atmos. Chem. Phys.*, 8, 2895–2932, <https://doi.org/10.5194/acp-8-2895-2008>, 2008.

2305 *Zhang, Y., Zhang, X., Wang, K., Zhang, Q., Duan, F., and He, K.: Application of WRF/Chem over*
 2306 *East Asia: Part II. Model improvement and sensitivity simulations, Atmos. Environ.*, 124, 301–
 2307 *320, https://doi.org/10.1016/j.atmosenv.2015.07.023*, 2016.

2308 *Zhao, B., Liou, K., Gu, Y., Li, Q., Jiang, J. H., Su, H., He, C., Tseng, H.-L. R., Wang, S., and Liu,*
 2309 *R.: Enhanced PM_{2.5} pollution in China due to aerosol-cloud interactions, Sci. Rep.*, 7, 1–11,
 2310 <https://doi.org/10.1038/s41598-017-04096-8>, 2017.

2311 *Zhou, C., Zhang, X., Gong, S., Wang, Y., and Xue, M.: Improving aerosol interaction with clouds*
 2312 *and precipitation in a regional chemical weather modeling system, Atmos. Chem. Phys.*, 16, 145–160,
 2313 <https://doi.org/10.5194/acp-16-145-2016>, 2016.

2314 *Zhu, J., Wang, S., Wang, H., Jing, S., Lou, S., Saiz-Lopez, A., and Zhou, B.: Observationally*
 2315 *constrained modeling of atmospheric oxidation capacity and photochemical reactivity in*
 2316 *Shanghai, China, Atmos. Chem. Phys.*, 20, 1217–1232, [https://doi.org/10.5194/acp-20-1217-](https://doi.org/10.5194/acp-20-1217-2020)
 2317 [2020](https://doi.org/10.5194/acp-20-1217-2020), 2020.

2318 *Zhu, J., Chen, L., Liao, H., Yang, H., Yang, Y., and Yue, X.: Enhanced PM_{2.5} decreases and O₃*
 2319 *increases in China during COVID-19 lockdown by aerosol-radiation feedback, Geophys. Res.*

Formatted: Font: Italic, Font color: Blue

Deleted: Womack, C. C., Manfred, K. M., Wagner, N. L., Adler, G., Franchin, A., Lamb, K. D., Middlebrook, A. M., Schwarz, J. P., Brock, C. A., and Brown, S. S.: Complex refractive indices in the ultraviolet and visible spectral region for highly absorbing non-spherical biomass burning aerosol, *Atmos. Chem. Phys.*, 21, 7235–7252, <https://doi.org/10.5194/acp-21-7235-2021>, 2021.

Formatted: Font: Italic, Font color: Blue

Formatted: Font: Italic, Font color: Blue

Formatted: Font: Italic, Font color: Blue, Subscript

Formatted: Font: Italic, Font color: Blue

Deleted:

Wu, Y., Cheng, T., Liu, D., Allan, J. D., Zheng, L., and Chen, H.: Light absorption enhancement of black carbon aerosol constrained by particle morphology, *Environ. Sci. Technol.*, 52, 6912–6919, <https://doi.org/10.1021/acs.est.8b00636>, 2018.

Xie, B., Fung, J. C. H., Chan, A., and Lau, A.: Evaluation of nonlocal and local planetary boundary layer schemes in the WRF model, *J. Geophys. Res. Atmos.*, 117, <https://doi.org/10.1029/2011JD017080>, 2012.

Formatted: Font: Italic, Font color: Blue

Deleted: Xu, D., Ge, B., Chen, X., Sun, Y., Cheng, N., Li, M., Pan, X., Ma, Z., Pan, Y., and Wang, Z.: Multi-method determination of the below-cloud wet scavenging coefficients of aerosols in Beijing, China, *Atmos. Chem. Phys.*, 19, 15569–15581, <https://doi.org/10.5194/acp-19-15569-2019>, 2019.

Zhang, S., Sarwar, G., Xing, J., Chu, B., Xue, C., Sarav, A., Ding, D., Zheng, H., Mu, Y., and Duan, F.: Improving the representation of HONO chemistry in CMAQ and examining its impact on haze over China, *Atmos. Chem. Phys.*, 21, 15809–15826, <https://doi.org/10.5194/acp-21-15809-2021>, 2021.

Deleted: Zheng, B., Zhang, Q., Zhang, Y., He, K. B., Wang, K., Zheng, G. J., Duan, F. K., Ma, Y. L., and Kimoto, T.: Heterogeneous chemistry: a mechanism missing in current models to explain secondary inorganic aerosol formation during the January 2013 haze episode in North China, ...

Formatted: Indent: Left: 0 cm, Hanging: 2 ch, First line: -2 ch, Don't adjust right indent when grid is defined, Don't adjust space between Latin and Asian text, Don't adjust space between Asian text and numbers

Deleted: